パワーエレクトロニクス励磁のためのアモルファス材の試作

濱島拓未、竹内恒博、藤崎敬介
（豊田工業大学）

Trial Manufacturing of Amorphous Material for Power Electronics Excitation

Takumi Hamashima, Tsunehiro Takeuchi, Keisuke Fujisaki
(Toyota Technological Institute)

電気モータの電気自動車応用に端を発し、その傾向が機関車、船、飛行機といった移動手段すべへの適用検討が進められている。移動に必要な可変速技術は、パワーエレクトロニクス励磁においてモータにて初めて実現可能とし、その傾向は十数年後には電気エネルギーの８割を介して制御されるといわれている。こうしたパワーエレクトロニクス技術において僅々の技術課題となっているのが高周波大電力のための磁性材料である[1]。例えばMHz程度の周波数をMW程度の大電力に対し変圧器を用いようとすると、少なくともμm厚み程度以下の鋼板を量産化すべきともいえる[2]。単にロールで急冷しても20 μm厚程度が限界といわれているので、アモルファス材のガラス転移点に着目した[3]。そこで今回、鉄合金($Fe_{78}Si_9B_{13}$)を単ロールで急冷しアモルファス材を作り、その後圧延にて薄くすることを試み、その磁気特性を計測した[4]。ガラス転移温度（420℃）前後にて300 Maを10分程度圧下し鋼板厚みを1-2割程度薄くなった（図１参照）。10 kHzでの磁気計測をしたところ、市販のアモルファス材(2605SA1:日立金属社製）より鉄損を小さくすることができた（図２参照）。

参考文献

1) 藤崎敬介「パワーエレクトロニクスで励磁される磁性材料」第41回日本磁気学会学術講演会　S-2,シンポジウム，パワーエレクトロニクスで励磁される磁気・磁性材料の研究の必要性，平成29年9月22日，九州大学.
2) 藤崎敬介「ミクロ材料電磁界数値解析による高周波軟磁性材料の形状と損失特性」電気学会マグネティックス・リニアドライブ・日本磁気学会合同研究会資料，MAG-14-208, LD-14-100, 2014.12.
3) T. Takeuchi et al., Local atomic arrangements and electronic structure of the Zr-Ni-Al bulk metallic glass -Analysis by use of the relevant crystals – Mat. Sci. Engng. A, 449-451 pp.559-604 (2007).
4) 濱島拓未「パワーエレクトロニクスに応用可能な軟磁性材料の開発」豊田工業大学卒業論文,2018.3

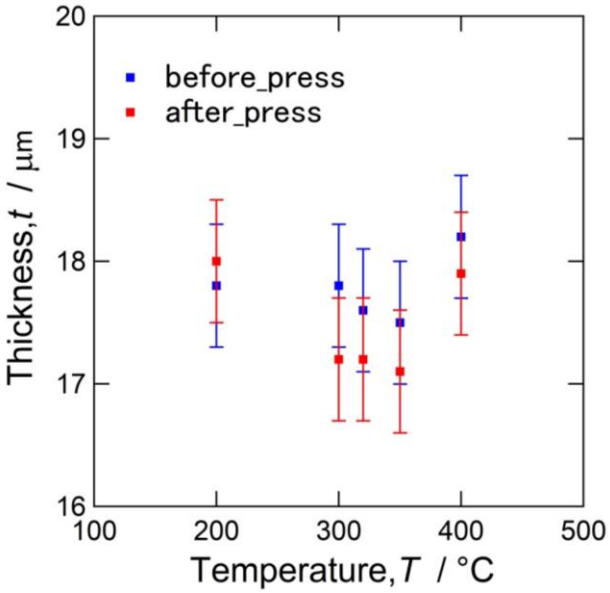

図１．圧下による鋼板厚みの変化

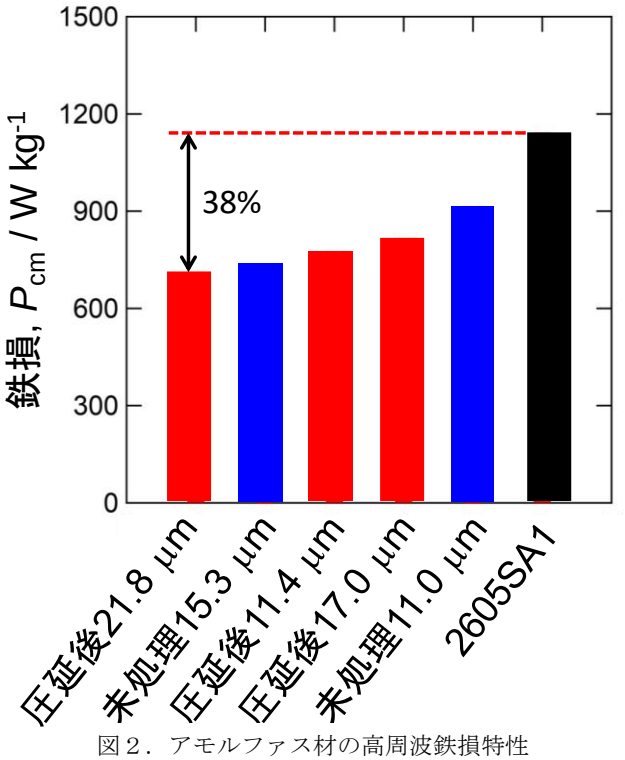

図２．アモルファス材の高周波鉄損特性
(10 kHz)

パワーエレクトロニクス励磁のための対向ターゲット式スパッタによる1μm厚鋼帯の試作

高村陽太*，小川良正*，古我城航*，中川茂樹*，藤﨑敬介**
*東京工業大学電気電子系，**豊田工業大学

Fabrication of 1-μm-thick CoFeB steel strips for power electronics excitation

Y. Takamura*, Y. Ogawa*, W. Koganoki*, S. Nakagawa*, K. Fujisaki**
Dept. of Electric and Electronic Eng., Tokyo Inst. of Tech., **Toyota Technological Inst.

背景

パワーエレクトロクス技術の進展で電力：MW クラス、周波数：MH z 程度といった高周波・大容量化の実用化が検討され始め、μm 厚み程度以下の鋼帯の磁気特性の把握が求められている [1]．従来の鋼帯作製技術では，薄層化に限界があった．一方の集積エレクトロニクスで用いられる真空成膜法 [2]では，数十 nm の薄さの成膜を得意とするため，μm オーダーの成膜はほとんど試されてこなかった．本研究では，真空薄膜作製技術の一つであるスパッタ法を用いて，1μm 厚鋼帯の試作に成功したので報告する．

作製方法

鋼帯は対向ターゲット式スパッタ法によりガラス基板上に作製した．まず，ガラス基板をアセトンとエタノールを用いてそれぞれ 10 分間超音波洗浄を 10 分間行った．基板を真空チャンバーに導入後，背圧が 1.5×10^{-4} Pa に達したところで，Ar ガスを導入し，Ar 分圧 0.1 Pa の下，1 時間 30 分間スパッタ成膜を行った．成膜速度は 12 nm/分であった．ターゲットは，mol 比で Fe:Co=7:3 の合金上に B チップを乗せたものを使用した．

結果

作製した FeCoB 鋼帯は，約 1μm という厚みにも関わらず，基板からの剥離や皺は確認されなかった．(図 1 挿入写真)このことは，さらなる厚膜化や多層構造化が可能であることを示唆している．また，鏡面をしていたことから，平坦な表面を持っていると考えられる．膜厚が 1.1μm であることは，試料を成膜装置の試料台にカプトンテープで貼り付けた跡の段差を実測し，確認している．

図 1 に試料振動型磁力計で測定した直流磁場に対する *B-H* 特性を示す．飽和磁束密度と残留磁束密度は，それぞれ，2.3 T と 0.7 T だった．

X 線回折による結晶構造解析から，CoFeB 鋼帯が(110)配向した体心立方格子を形成していることを確認した．格子定数は，0.286 nm であった．

また，膜の組成が，$(Fe_{0.7}Co_{0.3})_{0.93}B_{0.07}$ であることも誘導結合プラズマ発光分析 (ICP-OES)法を用いて分析した．

今回の結果は，真空成膜法を用いて 1μm の鋼帯が作製可能であることを示している．当日は，交流磁場に対する応答測定の結果等も含め発表を行う．

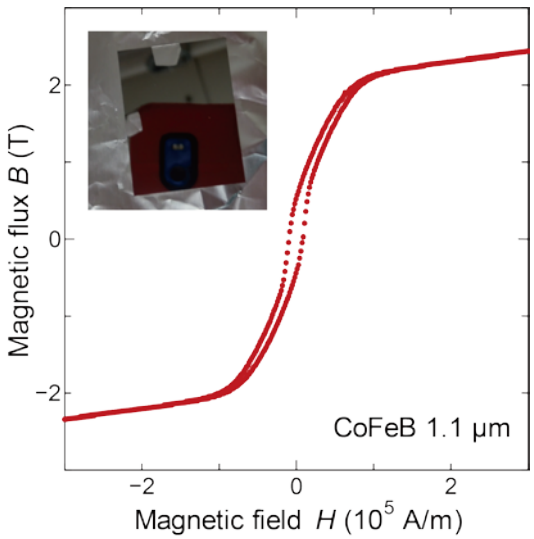

Fig. 1. DC magnetic hysteresis loops for a 1-μm-thick CoFeB steep strip on a glass substrate. The inset is the photograph of the steep strip.

参考文献

1)　藤﨑敬介「パワーエレクトロニクスで励磁される磁性材料」第 41 回日本磁気学会学術講演会　S-2,シンポジウム，パワーエレクトロニクスで励磁される磁気・磁性材料の研究の必要性，平成 29 年 9 月 22 日，九州大学.

2)　中川茂樹「斜方入射スパッタ粒子を利用して作製した高異方性磁界を有する FeCoB 膜」日本磁気学会誌まぐね, **7**, 26, (2011).

軟磁性金属扁平粉末を用いた高周波電源用薄型磁心材料の開発

御子柴 駿，嶋 博司，茶谷 健一
（株式会社　トーキン）

Soft magnetic metal flake composite suitable for high frequency, low profile power supply.

S. Mikoshiba, H. Shima, K. Chatani
(TOKIN Corporation)

はじめに

MPU や GPU など高性能プロセッサの性能向上に伴う供給電流の増加は著しく，DC-DC コンバータからプロセッサへの給電経路で発生するジュール損失の削減が課題となっている．損失削減の手法として，プロセッサの直下やパッケージに DC-DC コンバータを形成し，給電経路を短縮することによる消費電力削減が挙げられる．ここでチョークコイルは DC-DC コンバータを構成する部品の中で大きな体積を占めるため，プロセッサの直近に配置するためには，コイル磁心の小型・薄型化は必須である[1]．スイッチング周波数を MHz 超として構成部品を小型・薄型化することが考えられるが，フェライト系材料や従来の金属系圧粉体などは一般に脆性を示すため，割れ等の問題を生じ薄型化に限界がある．

そこで本報告では，薄型磁心を実現するために，表皮深さ程度の厚さを持つ扁平状粉末を高充填成形した磁心の磁気特性について報告する．

実験方法

ガスアトマイズ法で作製したセンダスト粉末(Fe-Si-Al)を，ボールミルにて鍛造し扁平状粉末を用意した．扁平粉末の配向にはドクターブレード法を採用し，扁平粉末とシリコーンレジン，増粘剤，溶剤を混合して得たスラリーをシート状に成形した．得られたシートに加圧成型と熱処理を施し，扁平粉末を一様に配向させた磁心を作製した．評価に使用する磁心の寸法は外径 26 mm×内径 16 mm×厚さ 0.5 mm とした．初透磁率はインピーダンスアナライザ，鉄損は交流 B-H アナライザ，磁化特性は直流 B-H アナライザで測定した．また構造観察には走査電子顕微鏡(SEM)を用いた．

実験結果

Fig. 1 に平均長径 40 μm，平均厚さ 1.5 μm に鍛造した扁平粉末を用いて作製した磁心の断面図を示す．扁平粉末の充填率は 70 vol. %を示し，扁平粉末の一様な配向が確認された．また扁平粉末が交互に積み重なった構造を有するため，面直方向に亀裂が進展しにくいと考えられる．すなわち曲げ応力に対し靭性を示し，薄型磁心に適した構造であると推察される．

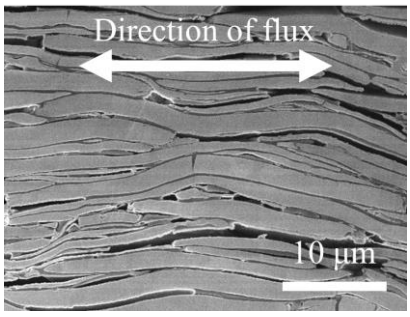

Fig. 1　Cross section of flake composite core. The average length of flake is 40 μm, thickness is 1.5 μm.

Fig. 2 に上記磁心の複素透磁率 μ', μ''を示す．μ'は 280 の値を 4 MHz 程度でも維持しており，既存の金属系圧粉磁心よりも優れた軟磁気特性を有している．これは数 MHz の周波数で想定される表皮深さ程度の厚さを持つ扁平粉末を，磁束の方向に対し一様に配向させたことによるうず電流の抑制と，充填率 70 vol. %の高充填を同時に実現できたためだと考えられる．

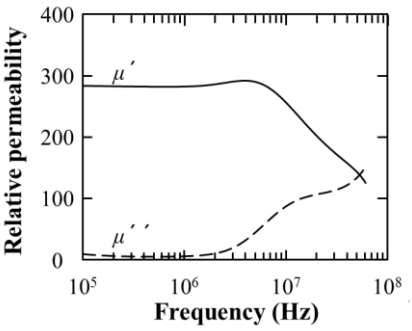

Fig. 2　The relative permeability of flake composite core in Fig. 1.

本磁心の構造，扁平粉末の厚さと鉄損の関係については当日詳細に報告する．

参考文献

1)　F. C. Lee et al., *IEEE Trans. Power Electron.*, **28**, 4127-4136 (2013).

大電流用低背インダクタの開発

○嶋博司、御子柴駿、茶谷健一
（株式会社トーキン）

Development of low height inductor for high current

H.Shima, S.Mikoshiba, K.Chatani
(TOKIN Co.)

はじめに

近年、FPGA やサーバー用プロセッサを駆動する DC/DC コンバータにおいて、低電圧高電流化、スイッチングの高周波化が求められている。またこれら DC/DC コンバータに搭載されるインダクタにおいても、大電流対応、損失低減が求められている。

今回、軟磁性金属扁平粉を含む磁心(扁平粉磁心)を用いてインダクタを作製し、既存のインダクタとの特性比較を行った。その結果、扁平粉磁心を用いたインダクタが低背化に適することが明らかとなった。

実験方法

扁平粉磁心の外周に金属導体を配置・接合した構造(Fig.1)、扁平粉磁心を基板に埋め込んだ構造(Fig.2)のインダクタを作製した。これらのインダクタについて直流重畳特性(Fig.3)、直流電気抵抗を測定し既存のインダクタとの性能比較を行った。

Fig.1 扁平粉磁心を用いたインダクタ

実験結果

インダクタの特性を比較するにあたり①インダクタンス L、②許容最大電流 Isat、③直流電気抵抗値を DCR とし、インダクタの性能指標を

$$L \times Isat / DCR$$

で定義した。

扁平粉磁心を用いたインダクタは、特にインダクタ高さの制限が大きい場合に優れた特性を示した。これは今回作製したインダクタの構造がラテラルフラックス型であるためと考えられる [1]。

また基板に内蔵した場合、省スペース化が可能になる他、プロセッサ直下にインダクタを配置することで、基板パターンによる銅損も削減することができる。

以上より、インダクタの低背化設計において扁平粉磁心を用いたインダクタが優位性を示すと言える。

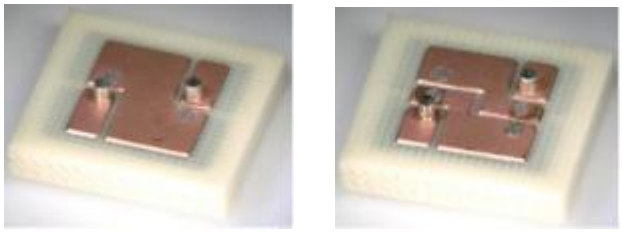

Fig.2 扁平粉磁心を基板に内蔵したインダクタ
2 ターン(左)、3 ターン(右)

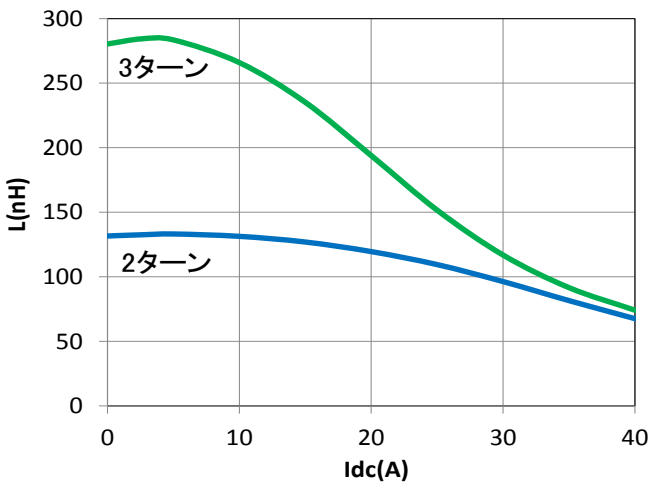

Fig.3 基板内蔵型インダクタの直流重畳特性

参考文献

1) Qiang Li, Fred C. Lee, “High Inductance Density Low-Profile Inductor Structure for Integrated Point-of-Load Converter”, 2009 IEEE Applied Power Electronics Conference and Exposition (APEC), Washington, District of Columbia, Feb. 15 – 19, 2009, pp. 1011 – 1017.

LEDストロボ照明による方向性電磁鋼板の励磁状態磁区観察

小田切 雄介、柳沢 栄二、目黒 栄、斉藤 伸*　（ネオアーク株式会社、*東北大学）

Strobe method magnetic domain observation of
oriented electrical steel sheet in condition of excitation using LED light source

Y. Odagiri, E. Yanagisawa, S. Meguro, S. Saito*　(Neoark Corporation, *Tohoku University)

はじめに

近年、地球温暖化対策として低炭素社会実現のために様々な取り組みが行われている。電磁鋼板は変圧器やモーターのコア材として幅広く活用されており、その性能改善はエネルギー利用効率上昇に直結する。電磁鋼板の磁気特性把握の手法としては商用周波数での実働状態における磁区観察が有用である。我々はこれまで磁気光学 Kerr 効果を利用した cm オーダ領域の広視野磁区観察装置の開発を行ってきた [1]。一般に商用周波数励磁下で磁区観察を行うためには、おおよそ 1000 fps 以上の高速度カメラを用いる必要がある。しかし、早いフレームレートにおける観察では 1 フレームの露光量が微弱となり、特に広視野観察において品位の高い観察像を得ることが困難となる。そこで我々はパルス駆動 LED を光源としたストロボ法を用いて商用周波数駆動における電磁鋼板の動的磁区観察を可能とする装置開発を行ったので報告する。

観察原理と装置構成

Fig. 1 に今回開発したストロボ法を適用した磁区観察装置のブロック図を示す。2 チャンネルのファンクションジェネレータを用い、一つのチャンネルで 50 Hz の正弦波信号を出力し、その信号を元に励磁用電源で交流磁場を発生させた。もう一つのチャンネルではパルス信号を出力して光源のパルス駆動を行った。光源を短時間点灯することで、高速な磁化挙動中の点灯時の励磁タイミングでの磁区像を切り出すことが可能となり、2 チャンネル間の位相差を変更していくことで磁区変化の撮像が可能となる。

光源には白色 LED を採用した。LED の点灯時間は 200 μsec とし、観察に用いるカメラのシャッター速度を 0.5 sec とした。約 25 発のパルスにより得られる光学情報を積算することで磁区像を取得した。試料を商用周波数で励磁するためにパーマロイコアの電磁石を製作した。この電磁石では 100 V、10 A 出力の励磁用電源と組み合わせ、60 Hz の周波数において 1 kOe 振幅の交流磁場を発生可能である。

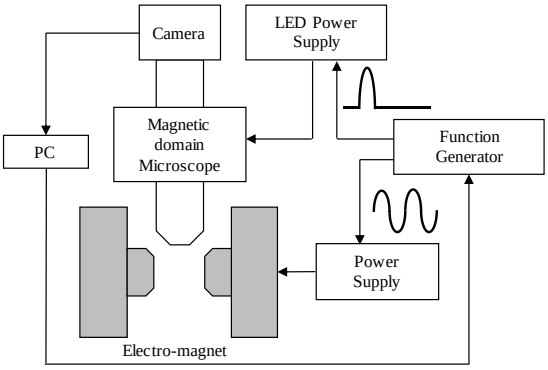

Fig.1　Block diagram of new developed equipment with stroboscopic irradiation by LED.

観察結果

Fig. 2 に方向性電磁鋼板の観察結果を示す。周波数 50 Hz、磁場振幅 800 Oe にて試料を励磁し、磁場がほぼ 0 Oe となるタイミングで像観察した。磁壁が明瞭な領域と不明瞭な領域が確認できる。これは 25 回の観察像において磁壁移動の再現性に分布があることを示唆している。このように商用周波数励磁での時間分解磁区観察は、比較的低い周波数で励磁した場合の磁化過程の再現性やヒステリシス損失の解析に有用な知見を与えるといえる。講演では、アモルファスリボンについての観察結果も報告する予定である。

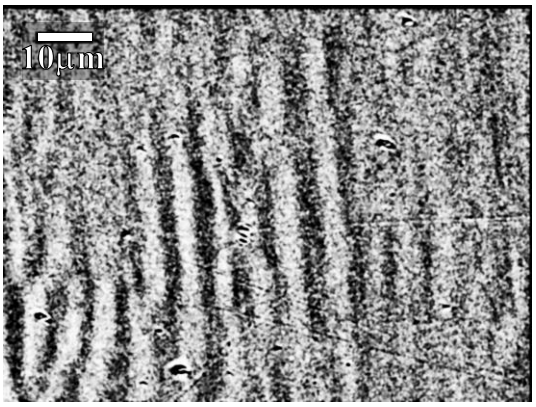

Fig. 2　Magnetic domain of electrical steel with applying the magnetic field of 50 Hz.

参考文献

1)　S. Meguro et al.: 28th *Ann. Conf. Magn. Soc. Jpn.*, 24aF-9 (2004).

自己フラックス法を用いた六方晶フェライト単結晶の作製

佐保拓未、柿崎浩一、神島謙二
(埼玉大学)

Single crystal growth by self-flux method of hexagonal ferrites

T. Saho, K. Kakizaki, K. Kamishima
(Saitama Univ.)

1. 緒言

六方晶フェライトは、S ブロック($(2MeFe_2O_4)^{0\pm}$, $(2Fe_3O_4)^{2+}$)、R ブロック($(BaFe_6O_{11})^{2-}$)および T ブロック($(Ba_2Fe_8O_{14})^{0\pm}$)の積層構造となっている(Me は二価遷移金属イオン)。これらのブロックの組み合わせにより、様々な構造を形成する。その構造に応じて硬磁性材料にも高周波軟磁性材料にもなりうる。[1] 本研究では、フラックス法を用いて 6 種類の既知構造の六方晶フェライト単結晶を作製し、その作製条件および磁気特性を調査した。

2. 実験方法

試料は自己フラックス法によって作製した。フラックスとして BaB_2O_4 (T_m = 1105°C)を選択した。原料は $BaCO_3$, ZnO, α-Fe_2O_3, B_2O_3 を用いた。六方晶フェライトの化学量論組成通りに秤量し、この組成とフラックスが 25 : 75 (75 mol%), 50 : 50 (50 mol%), 75 : 25 (25 mol%)のモル比になるように秤量した。これらを混合し、白金るつぼに充填した。1250°C で 5 時間保持した後、10°C/h で 1050°C まで徐冷し、1050°C からは放冷した。生成物から酸洗浄によりフラックスを除去し、六角板状の単結晶試料を得た。この試料を、大きさによって > 1, 1~0.3, < 0.3 mm に分けて回収した。得られた試料の結晶相は、粉末 X 線回折(XRD)を用いて同定し、磁気特性は振動試料型磁力計(VSM)を用いて調査した。

3. 結果と考察

図 1 は各組成で作製した試料の X 線回折図を示す。単結晶の大きさにはばらつきがあったものの、目的の単結晶はすべて得られた。

図 2 は各試料の熱磁気曲線である。M 型と Y 型は参照データと近いキュリー温度が得られた。[2] Z 型は M 型と Y 型が積層した構造となっており、キュリー温度はそれらの中間の値となった。また、X 型と U 型はそれぞれ M 型と W 型または Z 型の中間の積層構造となっているため、キュリー温度も各フェライトの中間の値が得られた。

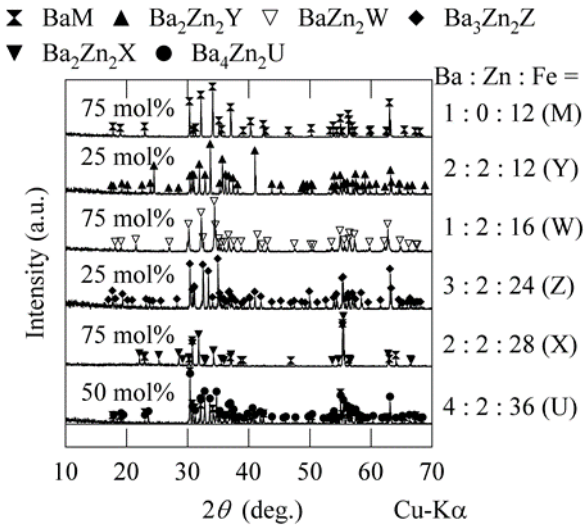

図 1. 組成の異なる各試料の X 線回折図

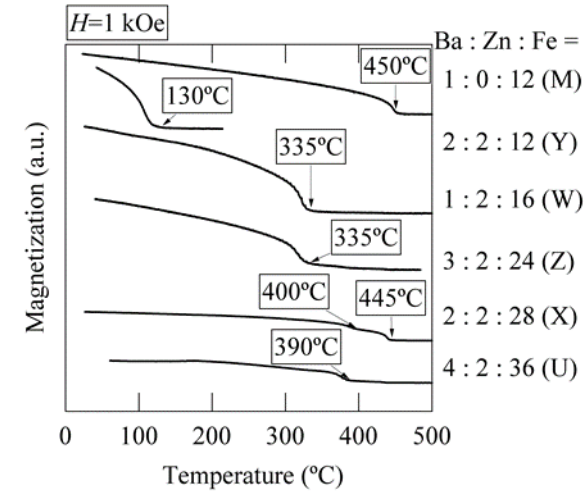

図 2. 組成の異なる各試料の熱磁気曲線

R ブロックと S ブロックのみで構成される構造はフラックスが 75 mol%で、T ブロックを含むものはフラックスが 25, 50 mol%で良質な単結晶が得られた。これは、R ブロックからなる構造と T ブロックからなる構造の溶解度が異なっており、T ブロックからなる構造の方が、溶解度が高いためであると考えられる。

六方晶フェライトに含まれるブロックにより、生成のし易さに違いがあることが明らかになった。この結果より、さらに複雑な積層構造をもつフェライト[3] を作製できる可能性がある。

参考文献

1) 平賀貞太郎 他, フェライト 丸善株式会社 (1986) 6, 18.
2) 近角聡信 他, 磁性体ハンドブック 朝倉書店 (1975) 636~644.
3) J. A. Kohn and D. W. Eckart, Zeit. Krist., 119 (1964) 454.

エピタキシャル bcc-$Fe_{100-x}Co_x$ 合金薄膜の回転磁界中における磁歪挙動

芹澤伽那[1,2]・川井哲郎[1]・大竹充[1]・二本正昭[2]・桐野文良[3]・稲葉信幸[4]
([1]横浜国大，[2]中央大，[3]東京藝大，[4]山形大)

Magnetostriction Behaviors of $Fe_{100-x}Co_x$ Alloy Epitaxial Thin Films under Rotating Magnetic Fields

Kana Serizawa[1,2], Tetsuroh Kawai[1], Mitsuru Ohtake[1], Masaaki Futamoto[2], Fumiyoshi Kirino[3], and Nobuyuki Inaba[4]
([1]Yokohama Nat. Univ., [2]Chuo Univ., [3]Tokyo Univ. Arts, [4]Yamagata Univ.)

はじめに　Fe および Fe-Co 合金は代表的な軟磁性材料であり，トランスなどの電磁エネルギー変換機器からセンサーなどの磁気デバイスまで幅広く用いられている．これらの応用では，飽和磁化や保磁力などの基本磁気特性に加え，磁歪特性の制御もしばしば要求される．我々は，これまで，結晶方位が異なる MgO 単結晶基板上に $Fe_{70}Co_{30}$（at. %）合金膜をエピタキシャル成長させ，その磁歪特性を回転磁界を用いて調べてきた[1]．本研究では，Co/Fe 組成を変化させることにより $Fe_{100-x}Co_x$ 合金膜を形成し，組成が磁歪挙動に及ぼす影響について系統的に調べた．

実験結果　いずれの組成においても，Mg(001)，MgO(110)，MgO(111)/Al_2O_3(0001)基板上には，それぞれ，bcc(001)単結晶，bcc(211)双結晶，bcc(110)複合エピタキシャル膜が形成された．また，磁化曲線を測定した結果，Fe，$Fe_{70}Co_{30}$，$Fe_{50}Co_{50}$ 膜の順に磁気異方性が減少する傾向が認められた Fig. 1(a-1)および(a-2)にそれぞれ Fe(001)単結晶膜の bcc[100]および bcc[110]方向に対して観察を行った磁歪の出力波形を示す．いずれの観察方向においても，低磁界強度では，磁気異方性により磁化と回転磁界方向が一致していないため[2]，Fig. 1(a-1)ではバスタブ状，Fig. 1(a-2)では三角状の波形が現れている．磁界強度の増加に伴い，磁化と磁界方向が一致し，正弦波に近づく傾向が認められる．Fig. 1(b)および(c)に $Fe_{70}Co_{30}$ および $Fe_{50}Co_{50}$ 膜の磁歪波形をそれぞれ示す．磁気異方性の減少に伴い，より低磁界強度で正弦波となっていることが分かる．また，1.2 kOe の磁界印加時の出力波形から求めた Fe，$Fe_{70}Co_{30}$，$Fe_{50}Co_{50}$ 膜の磁歪定数(λ_{100}, λ_{111})は，それぞれ，$(25\times10^{-6}, -24\times10^{-6})$，$(170\times10^{-6}, 11\times10^{-6})$，$(70\times10^{-6}, 62\times10^{-6})$となり，バルク結晶[3]と同様に $x = 30$ の組成付近で大きな λ_{100} が現れることが分かった．当日は，bcc(211)双結晶および bcc(110)複合膜の磁歪挙動についても報告する．

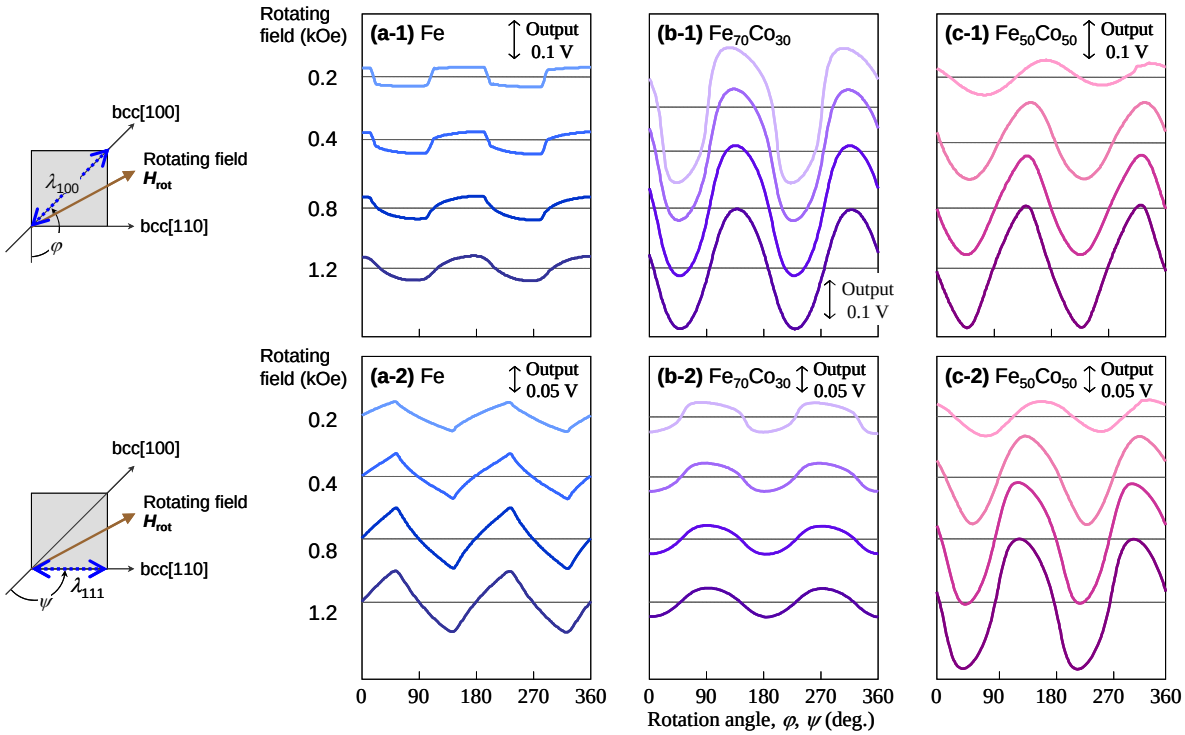

Fig. 1 Output waveforms of magnetostriction for bcc(001) single-crystal (a) Fe, (b) $Fe_{70}Co_{30}$, and (c) $Fe_{50}Co_{50}$ films measured parallel to (a-1)–(c-1) bcc[100] and (a-2)–(c-2) bcc[110] under different rotating magnetic fields.

参考文献

1)　芹澤伽那, 川井哲郎, 大竹充, 二本正昭, 桐野文良, 稲葉信幸: 第 41 回日本磁気学会学術講演会概要集, p.166 (2017).
2)　T. Kawai, T. Aida, M. Ohtake, and M. Futamoto: *J. Magn. Soc. Jpn.*, **39**, 181 (2015).
3)　近角聡信: 強磁性体の物理, p.122 (1963).

Thickness and growth temperature dependence of soft magnetic properties of (FeCo)-Si alloy thin films

K. Abe[1,2], Shuang Wu[1,3], Y. Ariake[1,2], I. Kanada[1,2], T. Mewes[1,3], G. Mankey[1,3], Y. Tanaka[2], C. Mewes[1,3], and T. Suzuki[1,4,5]

[1]Center for Materials for Information Technology, The University of Alabama, Tuscaloosa, AL 35487 USA
[2]Materials Development Center, TDK Corporation, Narita 286-0805, Japan
[3]Department of Physics and Astronomy, The University of Alabama, Tuscaloosa, AL 35487 USA
[4]Department of Metallurgical and Materials Engineering, The University of Alabama, Tuscaloosa, AL 35487 USA
[5]Department of Electrical and Computer Engineering, The University of Alabama, Tuscaloosa, AL 35487 USA

Iron-based crystalline alloys with low effective damping parameter have potential applications for future high-frequency devices. Recent work on Fe-Co-Al alloy thin films report an effective damping parameter as low as about 0.0004 for a composition of $Fe_{73}Co_{25}Al_2$ measured by FMR over a frequency range from 12 to 66 GHz.[1,2,3)] Although (FeCo)-Si alloy thin films have been extensively studied,[4,5)] very little information can be found in literature about the relation between effective damping parameter and structural properties. In this paper, the thickness and growth temperature dependences of soft magnetic properties of $(Fe_{75}Co_{25})_{95}Si_5$ alloy thin films are presented.

Multilayers of [Fe(0.35 nm)/$Fe_{66}Co_{34}$(1.1 nm)/Si(0.14 nm)] × N were sputter-deposited onto MgO (100) single crystal substrates using DC magnetron sputtering, where N is the number of repetitions. Deposition was carried out in Ar atmosphere of 4 mTorr. The substrate-deposition temperature T_s was varied from ambient to approximately 300 ℃. An in-plane field of 50 Oe was applied during deposition to induce a uniaxial magnetic anisotropy. A 5 nm thick Ru layer was over-coated to prevent oxidation. Structural analyses were performed by XRD and TEM. Measurements of magnetic properties were carried out by VSM and longitudinal MOKE. The magnetization dynamics was evaluated by ferromagnetic resonance (FMR) at room temperature over a frequency range from 12 to 66 GHz.

Figure 1 shows the dependence of (a) saturation magnetization M_s, (b) coercivity H_c, and (c) effective damping parameter α_{eff} on film-thickness d at different T_s. It is seen that M_s tends to decrease slightly with d from about 1,700 to 1,500 emu/cm^3. while H_c initially increases with d, and then decreases. The α_{eff} rapidly decreases with d, and then slightly increases for both the deposition temperatures.

The work is in part supported by the MINT-TDK collaboration program.

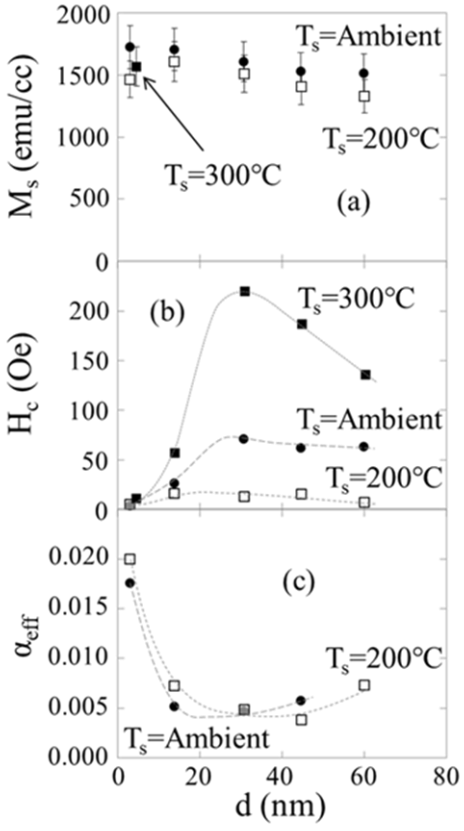

Fig. 1 Thickness dependence of (a) saturation magnetization M_s, (b) coercivity H_c, and (c) effective damping parameter α_{eff} for $(Fe_{75}Co_{25})_{95}Si_5$ films deposited onto MgO(100).

References

1) I. Kanada et al., AIP Advances, 7, 056105 (2017).
2) Y. Ariake et al., IEEE Trans. Magn., 53, 11 (2017).
3) Y. Ariake et al. AIP Advances 8, 056119 (2018).
4) M. Hayakawa et al., IEEE Trans. Magn., 23, 5 (1987).
5) L. Xi et al., Physica B 405,608 (2010).

有機金属分解法による亜鉛フェライトの合成と磁気特性

安達信泰、中田勇輔、太田敏孝
（名古屋工業大学）

Preparation and Magnetic Properties of $ZnFe_2O_4$ by MOD Technique

N. Adachi, Y. Nakata, T. Ota　(Nagoya Institute of Technology)

1.はじめに

$ZnFe_2O_4$は、可視光領域に透過性のあるフェライトの一つであり、反強磁性を示すことで知られている。最近、急冷法やPLD法により作製した$ZnFe_2O_4$結晶では、強磁性を示す報告がなされている[1,2]。我々は、有機金属分解法により、保磁力を示す$ZnFe_2O_4$薄膜が作製できることを見出した。もともとのイオン配置は、Zn^{2+}イオンが四面体位置、Fe^{3+}イオンが八面体位置にあるが、一部のFe^{3+}イオンが四面体位置に入ることでフェリ磁性の準安定相ができると考えられている。本研究では、熱処理結晶化過程を磁化の温度変化、磁気共鳴の実験を行い、結晶化過程の違いによる$ZnFe_2O_4$薄膜の磁気特性の変化を調べることを目的とした。

2. 実験方法

薄膜は、有機金属分解(MOD)法を用いて、シリカガラス基板上に作製した。溶液滴下後は、100℃で乾燥し、300℃で仮熱処理を行い、必要な膜厚まで、この工程を繰り返し、最後に、600℃で$ZnFe_2O_4$を熱処理結晶化させた。作製した試料に対し、XRDによる結晶の評価、SEMによる表面と断面と微構造観察、SQUIDとESRによる磁気特性の評価を行った。

3. 結果と考察

結晶化した薄膜は、単相の$ZnFe_2O_4$を示す多結晶回折ピークのみが観測され、二次相によるピークは観測されなかった。EDSによる組成分析ではZnやFeの濃度偏析が見られなかったことから、組成比の均一な膜を得ることが確認できた。Fig.1に作製した膜の1000 Oeでのfield cool時のM-T曲線を示す。自然放冷した膜では15 K付近にカスプが現れ、ネール点と考えられる転移が観測されたが急冷した膜では、低温での磁化率の減少は見られなかった。4KでのM-H曲線では、Fig.2に示すように700 Oe程度の保磁力を示す強磁性ヒステレシス曲線が観測され、急冷した膜は自然放冷した膜よりも大きな磁化が観測された。磁気共鳴のスペクトルの温度変化では、極低温領域では、ゼロ磁界で共鳴が起きている振る舞いが観測され、温度上昇とともに共鳴磁界が高磁場側にシフトする結果が得られた。反強磁性相と強磁性相が共存し、四面体位置のFe^{3+}イオン置換量が強磁性の原因と考えれば、熱処理過程でその割合を制御できる可能性が考えられる。

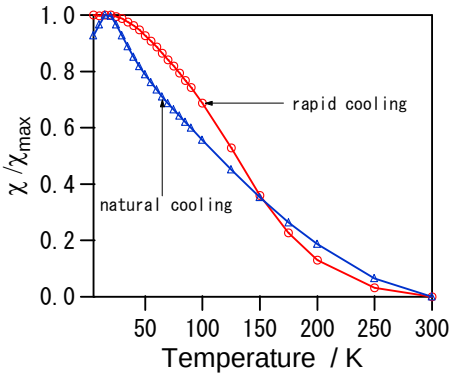

Fig.1 The field-cool M-T curve of $ZnFe_2O_4$ film under the magnetic field of 1000 Oe

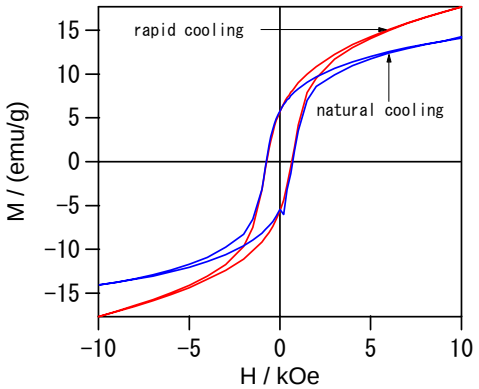

Fig.2. The H-H curves at 4 K of $ZnFe_2O_4$ films annealed at 600 ℃.

参考文献
1) K. TANAKA et.al. , J. Phys. Chem Solids Vol 59, No. 9, pp. 1611–1618 (1998)
2)N. Wakiya et.al. J. Mag. Mag. Mat. 310 (2007) pp.2546-2548

DES 浴から作製した Fe-Ni 膜の浴添加剤による軟磁気特性改善

柳井武志，山口知輝，森村隆夫，中野正基，福永博俊（長崎大学）
Improvement in soft magnetic properties of Fe-Ni films prepared in DES-based plating baths with additives
T. Yanai, T. Yamaguchi, T. Morimura, M. Nakano, H. Fukunaga (Nagasaki University)

はじめに

電解めっき法は，①高速成膜可能，②装置が簡素，③常温・常圧下での成膜が可能，などの利点を有しており，磁性膜作製の手法として魅力的な方法の一つである。磁性めっき膜に関する報告は，これまでに多くの研究者によってなされているが一般的に，水を溶媒とするものが多い。水は安価で扱いやすい溶媒であるが，比較的低電位で水の電気分解が生じるため，例えば希土類元素のような析出電位が大きく卑な元素を析出させることは困難である。そこで我々は，水に替わる新しい溶媒としてイオン液体の一種である深共晶溶媒（DES: Deep Eutectic Solvent）に着目し，検討を重ねてきた。最近の DES 浴から作製した Fe-Ni 膜に関する研究で，一級アミンを浴添加することで Fe-rich 組成膜にて大きく軟磁気特性が改善できることがわかってきた[1-2]。本稿では，一級アミン添加剤としてアミド硫酸アンモニウムを用いた際の結果について報告する。

実験方法

10 g の塩化コリンと 10 g のエチレングリコールを無色透明になるまで撹拌したものを DES とした。この DES に塩化鉄と塩化ニッケルを合計で 15 g 加えた。膜の組成は，塩化鉄と塩化ニッケルの重量比によって任意の組成に調整した。このめっき浴にアミド硫酸アンモニウムを 3 g 添加した。浴温度は 100°C，電流密度は 66.7 mA/cm^2 とし，Cu 基板上に Fe-Ni 膜を成膜した。

実験結果

Fig.1 に保磁力の Fe 組成依存性を示す。Fig.1 には，水溶媒の結果[3]およびマイクロマグネティックス理論で計算した保磁力の計算値も示している。Fig.1 より，DES 浴から作製した Fe-Ni 膜は Fe 組成の増加に伴い，保磁力が減少した。一方，水溶媒の結果および計算値は $Fe_{25}Ni_{75}$ 付近の組成で低保磁力を示しており，保磁力の Fe 組成に対する振る舞いが大きく異なることが了解される。Fig.2 に $Fe_{80}Ni_{20}$ 膜の TEM 像を示す。Fig.2 より，柱状の組織が形成されていることが了解される。このような柱状構造は Fe-poor な組成の膜では観測されなかった。よって，Fig.1 の保磁力の変化は Fe 組成の増加に伴い，ランダムな多結晶組織が柱状組織へ変化することが一つの要因として考えられる。Fe を多く含む組成領域で低保磁力を示す現象は結晶磁気異方性や磁気歪みからは予測できない DES 浴の特異的な現象である。本点に関しては現在も検討を継続しており，今後その要因を明らかにしていく予定である。

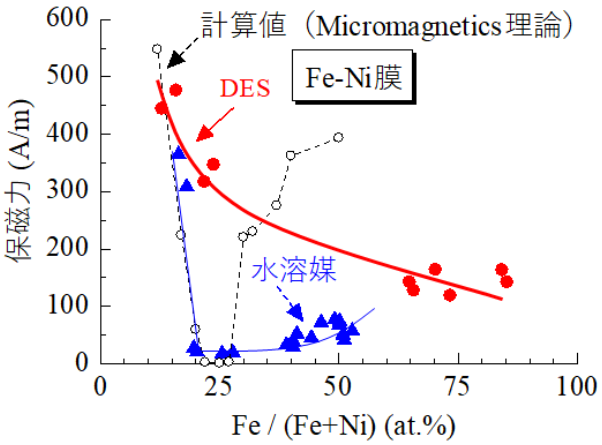

Fig.1 保磁力の Fe 組成依存性

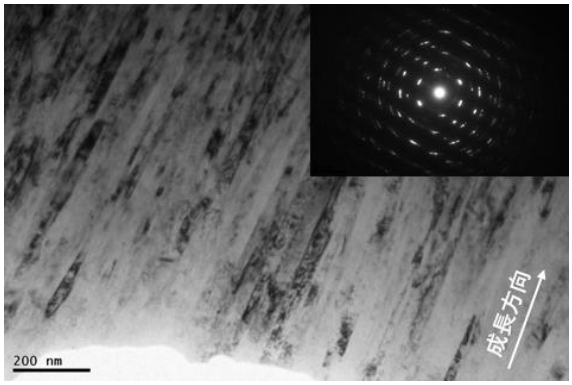

Fig.2 $Fe_{80}Ni_{20}$ 膜の TEM 像

参考文献

[1] T. Yanai, T. Yakaguchi *et al.*, *IEEE Trans. Magn.*, **53** (2017) #2004404.
[2] T. Yanai, T. Akiyoshi *et al.*, *AIP Advances*, **8** (2018) #056437.
[3] T. Shimokawa, T. Yanai *et al.*, *IEEE Trans. Magn.*, **48** (2012) 2907.

鉄系金属微粒子へのシリカコートに関する基礎検討

稲垣 悠太郎，杉村 佳奈子，藪 直希，佐藤 敏郎，曽根原 誠
（信州大学）

Basic investigation on silica coating iron-based metal particles

Y. Inagaki, K. Sugimura, N. Yabu, T. Sato, M. Sonehara
(Shinshu University)

はじめに

電気エネルギーの効率的な運用の要であるパワーエレクトロニクス分野では，高速スイッチング・低 ON 抵抗の特徴を有する SiC/GaN 次世代パワーデバイスの利用に注目が集まっている．SiC/GaN パワーデバイスを用いることで，高効率・小型軽量を両立したスイッチング電源の実現が望めるが，数 MHz 以上を駆動周波数とする磁心材料が Ni-Zn フェライトに限られているのが実情である．筆者らは MHz 帯磁心材料である鉄系メタルコンポジット磁心を提案した．磁心中において粒子を跨いで流れる渦電流による渦電流損失の増加を防ぐために粒子表面に高抵抗被膜を形成し，電気的に絶縁する必要がある．我々はこれまで，大気中熱酸化，シリカコーティング，酸溶液処理を提案した[1)-3)]．本稿では，シリカコーティングについて報告する．

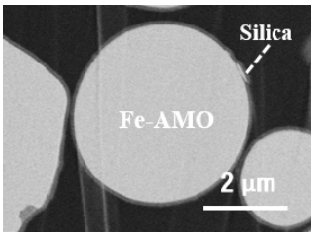

Fig.1 Silica coating on Fe-AMO(D_{50}=3.36 μm)

Table.1 Three kinds of Fe-AMO

	Fe-AMO		
Median diameter	3.36 μm	5.16 μm	11.13 μm
Specific surface area	0.454 m^2/g	0.312 m^2/g	0.204 m^2/g

実験方法

本稿では異なるメディアン径の鉄系アモルファス合金粉(以下 Fe-AMO)にシリカコーティングを行い，液相加水分解法(Stöber 法)を採用した．エタノール中に粉末を入れ，超音波洗浄機および攪拌棒を用いて粉末を分散させ，十分な処理時間コーティングを行うことにより粒子に被膜を形成した．

実験結果

Fig. 1 にシリカコーティング Fe-AMO の粒子の断面 SEM 像を示す．Fig. 1 より，シリカ被膜が形成されることが確認できる．Table 1 に 3 種類の Fe-AMO のメディアン径および比表面積を示し，Fig. 2 にそれぞれの Fe-AMO にシリカコーティングを行い，被膜の厚さを測長した結果を示す．横軸は粉末 1 g に対する TEOS の量を 0.04-0.32 [ml/g]の範囲で変化させた際の膜厚である．Fig. 2 より，何れの粒径の粉末においても膜厚は飽和し，粒径が小さいほど飽和領域の膜厚は厚くなることが分かる．また膜厚の線形領域において，同じ TEOS の量でも比表面積が小さいほど膜厚が厚くなることから，線形領域での膜厚は比表面積に依存することが分かる．以上より，シリカコーティングにより形成される被膜は，TEOS の量や粉末のメディアン径，比表面積を加味することで制御が可能であることが明らかになった．

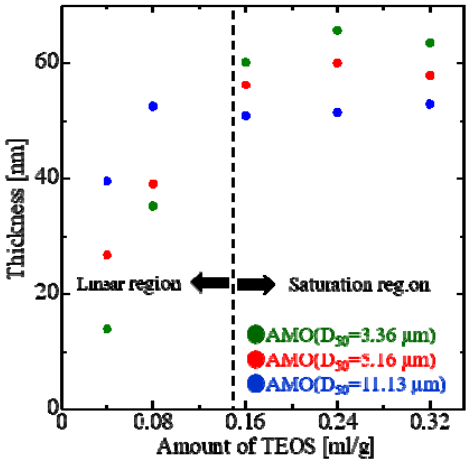

Fig.2 Silica coating on three kinds of Fe-AMO

参考文献

1) K. Sugimura, et al, *AIP Advances*, **6**, #055932 (2016).
2) K. Sugimura, et al, *Annual Conf. IEEJ Fund. and Mat.*, 5-B-p2-2 (2016).
3) N. Yabu, et al, *41th Annual Conf. Meeting Magn. Jpn.*, 21pc-8 (2017).

自然長格子(LaO)ZnPn (Pn=P, As, Sb)の弱い室温強磁性

高瀬浩一、下村大河、高野良紀
（日本大学理工学部）
Room temperature weak ferromagnetism of the natural superlattice (LaO)ZnAs
K. Takase, T. Shimomura, Y. Takano
(College of Science and Technology, Nihon Univ.)

はじめに

希土類層状オキシプニクタイド(LaO)ZnP は、ブロッキン層の LaO 層と伝導層の ZnPn 層が結晶の *c* 軸方向に交互積層した層状物質で、酸素は 4 つの La 原子に、Zn は 4 つの Pn 原子に四面体的に囲まれた構造を有している。Zn の 3*d* 軌道は 10 個の 3*d* 電子によって全て占められており、このため、この物質は磁性をもたない。

今回、我々は、Zn を欠損させることでホールを導入し、磁気モーメントの誘起を試みた。Zn を欠損させると、Pn 原子の *p* 軌道に不対電子が生じるか（c)、Zn の 3*d* 軌道に不対電子が生じる（d）と期待され、もし、うまく Zn に不対電子が生じるなら、これがもとで磁気モーメントが生じる期待される。逆に、(c)の場合だと、価電子帯を構成する *p* 軌道に不対電子が導入されるので、キャリアの導入により電気抵抗が減少すると考えらえる。

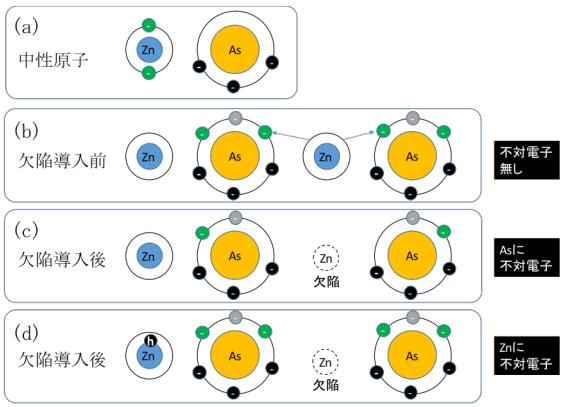

Fig. 1　Conceptual diagram of hole doping

実験方法

試料は全て多結晶体であり、固相反応法を用いて作成した。試料の磁化は MPMS を用い、電気抵抗は PPMS を用いて測定した。

実験結果

Fig. 2 に今回の試みの一例として、プニコゲンに P を選択した場合である(LaO)Zn_{1-x}P の電気抵抗の温度依存性（a）と室温での磁化の磁場依存性（*M*-*H*）（b）を示す。電気抵抗は Zn 欠損導入により著しく低下するが、温度依存性は全ての試料で半導体的なままである。一方、*M*-*H* カーブには、*x*=0.3 で小さなヒステリシスが観測され、強磁性が観測れた。

発表当日には、Pn=As, Sb の結果も紹介するとともに、室温で観測される弱い強磁性の起源について議論する。

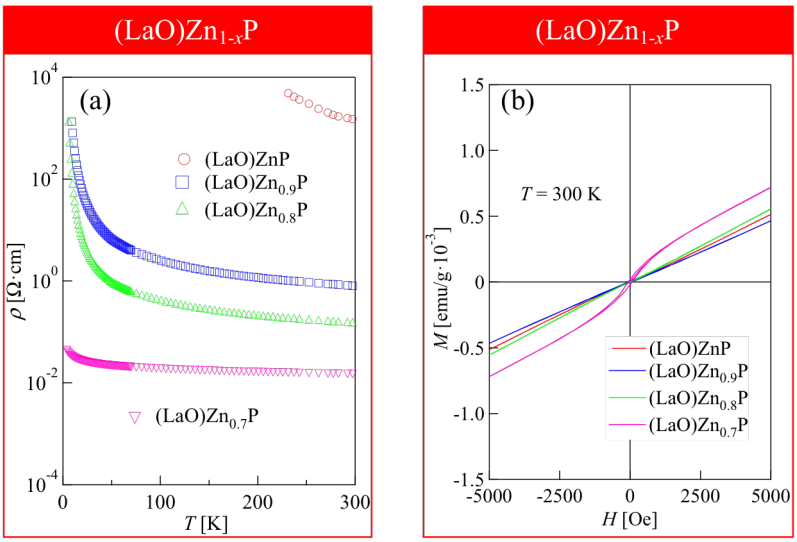

Fig. 2　Temperature dependence of electrical resistivity (a) and magnetic field dependence of magnetization at room temperature (b)

Issues with Micromagnetic Numerical Simulations of Magnetic Structures of Soft Magnetic Materials for Electric Vehicles

F. Akagi[1]
[1]Dept. of Applied Physics, Kogakuin Univ., Shinjuku 163-8677, Japan

1. Introduction

Ferromagnetic materials are used in the drive motors of electric vehicles. NdFeB magnets are used on the rotating part (or “rotor”) of drive motors and electrical steel is used on the stationary part (or “stator”). In terms of magnetic properties, NdFeB magnets are classified as hard magnetic material and electrical steel as soft magnetic material. Electrical steel has two magnetic characteristics. One is that iron loss (sum of hysteresis and eddy current losses) is low during transformation between electrical and magnetic energies. The other is that high magnetic flux densities are obtained even if low magnetic fields are applied to the soft magnetic materials. We previously reported that we performed micromagnetic numerical simulations of magnetic domain structures in electrical steel [1)]. Calculation models were assumed to be grain-oriented electrical steel (GOES) for transformer cores with an anisotropy field at 20 kA/m. Magnetization reversal in the GOES occurred by applying a DC magnetic field of 8 kA/m. This DC magnetic field was less than half of the anisotropy field but experimentally equals zero, which corresponds to the coercivity (H_c) of the GOES. Therefore, the DC magnetic field used for the micromagnetic numerical simulations was larger than expected. In this report, we describe issues with using electrical steel in simulation models, and we compare MH-loops between soft and hard magnetic materials to clarify what the issues with the micromagnetic numerical simulations for soft magnetic materials are.

2. Micromagnetic numerical simulation

In this simulation, a dynamic magnetic reversal process was calculated using the Landau–Lifshitz–Gilbert equation as follows:

$$\frac{\mathrm{d}M}{\mathrm{d}t} = -\gamma(M \times H_{eff}) + \frac{\alpha}{M_s}\left(M \times \frac{dM}{\mathrm{d}t}\right), \tag{1}$$

where, M is magnetization and M_s is saturation magnetization [2)]. H_{eff} is an effective field, which is the sum of an external, static, anisotropy, and exchange fields. γ is the gyromagnetic ratio and α is the damping factor.

In our calculations of MH-loops, a model of magnetic material contained 16×16×16 cubic cells that were 3 nm long. The M_s was 1.0 T, the intercell exchange stiffness constant was assumed to be 1.0×11^{-11} J/m, and the damping constant was 0.02. The cells have uniaxial magnetic anisotropy, which aligned in one direction. The anisotropy field (H_k) was changed from 10–300 kA/m. The external field was defined by a cosine function, of which the frequency was 25 MHz.

3. Results and discussions

Table 1 compares the magnetic characteristics of soft and hard magnetic materials. Magnetic domain wall width (σ) and exchange length (ρ) are given as

$$\sigma = \pi\sqrt{\frac{A}{K_u}}, \qquad \rho = \sqrt{\frac{A}{K_u}}, \tag{2}$$

where A is the exchange stiffness constant and K_u is the anisotropy constant. The soft magnetic materials are referred to as GOES and non-GEOS; the hard magnetic materials are referred to as NdFeB for motors and CoCr alloy for hard disk drives. The cell sizes of simulation models are defined by exchange length; the cell sizes must be equal to or less than the exchange length for the NdFeB and CoCr alloy. We must consider the cell size and magnetic domain width for

GOES or non-GEOS. The exchange length cannot be calculated and the cell size cannot be determined because the magnetic domain wall width and the exchange stiffness constant are unknown. If the magnetic domain wall width is on the order of 10 nm—which equals 100–150 atoms—the intercell exchange stiffness constant is 2×10^{-13} J/m and the exchange length is about 4.5 nm. Therefore, the cell size should be smaller than 4.5 nm. However, the number of the cell is needed more than 20,000 in the direction of magnetic domain width, because the magnetic domain width is over 100 μm for GEOS. Therefore, simulations of GEOS are very difficult because they are time-consuming and require a lot of memory. As the cell increases in size, simulations of the motions of the magnetic moments in the magnetic domain wall are not precise.

Next, we compared MH-loops between soft and hard magnetic materials to clarify what the issues with the micromagnetic numerical simulations of the soft magnetic materials are. The magnetic materials were assumed to be small, as mentioned in Chapter 2. Figure 1 shows the relationship between H_k and H_c, calculated from MH-loops. The graph in Fig. 1 shows that when the H_k was higher than or equal to 100 kA/m, the H_c was proportional to the H_k. When the H_k was lower than 100 kA/m, the H_c was about 30–40 kA/m. In particular, when the H_k was lower than 20 kA/m, the H_c was larger than H_k. This might be due to the equilibrium between the exchange and static magnetic fields.

We have to solve the above issues in order to simulate soft magnetic materials using a micromagnetic numerical simulation.

Table 1 Comparison of magnetic characteristics of soft and hard magnetic materials.

Magnetic material		Grain size	Magnetic domain width	Magnetic domain wall width (nm)	M_s (T)	K_u (J/m^3)	H_k (kA/m)	Exchange stiffness constant (J/m)	Exchange length (nm)	Cell size (nm)
Soft	GOES	1−2 cm (～10 μm)	> 100 μm	unknown	2	2×10^4	20	unknown	-	-
	Non-GOES		> 10 μm							
Hard	Nd-Fe-B	200−1000 (nm)	-	4.4	1.6	5×10^6	6000	1×10^{-11}	1.4	2
	CoCr alloy	< 10 (nm)	-	10.0	< 1.0	$> 1 \times 10^6$	2000	1×10^{-11}	3.2	1−10

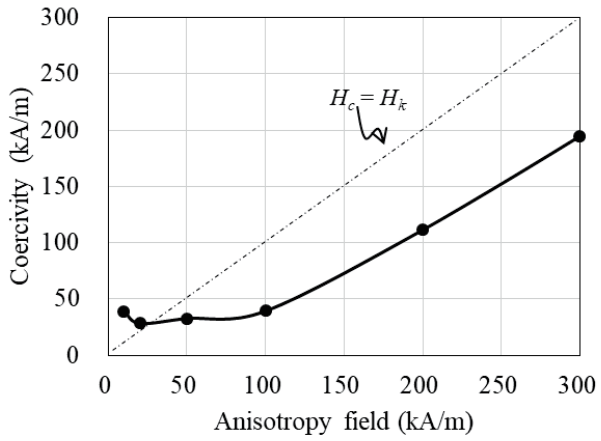

Fig. 1 Anisotropy field dependence of coercivity.

Acknowledgments

We thank Hitachi Corp. for providing us with the use of this simulator.

References

1) F. Akagi, K. Fujisaiki, The Papers of Joint Technical Meeting on “Rotating Machinery” and “Linear Drives” RM-17-045, LD-17-026, 2017, p. 19.

2) F. Akagi, J. Ushiyama, A. Ayano, and H. Miyamoto, “Head and Granular Media for Thermally Assisted Magnetic Recording for Recording Density of 6 Tb/in^2,” *IEEE Trans. on Magn.*,Vol. 49, Issue 7, 2013, p. 5667.

Polycrystalline Magnetic Field Analysis of Electrical Steel for Magnetic Multi-Scale

Keisuke Fujisaki
(Toyota Technological Institute)

Electrical steel is mainly used for electrical motor core or transformer due to high magnetic performance and mass production technology. It is polycrystalline material where each crystal has some magnetic domain with saturated magnetization. So it is said to be an important role between magnetic domain and electrical motor in magnetic multi-scale problem. Usually its calculation model of magnetic analysis should be carried out by magnetic domain model such as LLG or so. However, since electrical steel of polycrystalline has a lot of magnetic domains, when all the magnetic domains are considered for numerical calculation, mesh explosion problem will occur. So the polycrystalline of electrical steel should be modeled to avoid it. Here, static magnetic field analysis in finite element method is used for it in some assumptions that equivalent magnetic material constants are used in homogenized method and coordinate transform of magnetic flux density is used[1-3].

Figure 1 shows total coordinates in polycrystalline and local coordinates in each crystal. Magnetic anisotropy of each crystal is expressed in local coordinate and continuity of magnetic flux density is expressed in total coordinate[4]. So the coordinate transform between them is carried out. GO (grain oriented steel) material with 56 crystal grains in 80 mm^2 square are used for calculation in comparison with the measured magnetic property. Crystal orientations as α, β, γ angles defined in Fig. 1 are well organized and they are centralized within several degrees in average.

Figure 2 shows comparison of magnetic flux density distribution between 3D polycrystalline magnetic field analysis and distributed magnetic measurement[4]. Fig. 2 (a) is measured magnetic flux density by needle method with some square and Fig. 2 (b) is calculation one where magnetic flux density distribution as Fig. 3 (c) is averaged in some square of the needle method. The calculation result well expresses the measured one.

Figure 3 shows comparison of inclination angle of magnetic flux density vector $\vec{B}$ between 3D polycrystalline magnetic field analysis and distributed magnetic measurement[4]. Fig. 3 is the calculated inclination angle which is an angle between the easy magnetization direction of the polycrystalline and the magnetic flux density vector, and Fig. 3 (b) is α angle of each crystal grain. Magnetic flux density is expected to flow in polycrystalline in order to follow each crystal orientation. So angle distribution of Fig. 3 (a) and (b) are in good agreement.

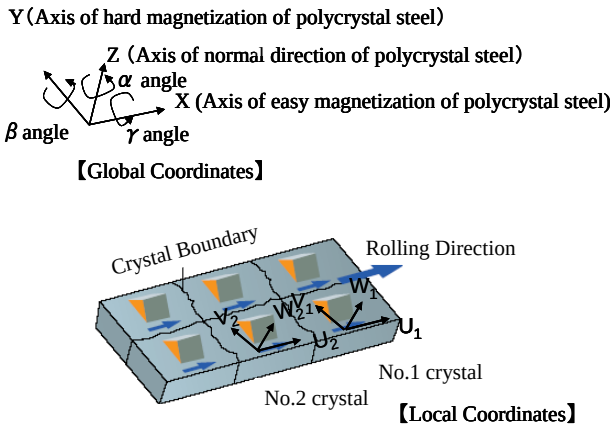

Fig.1. Total coordinates and local coordinates for polycrystalline magnetic field analysis.

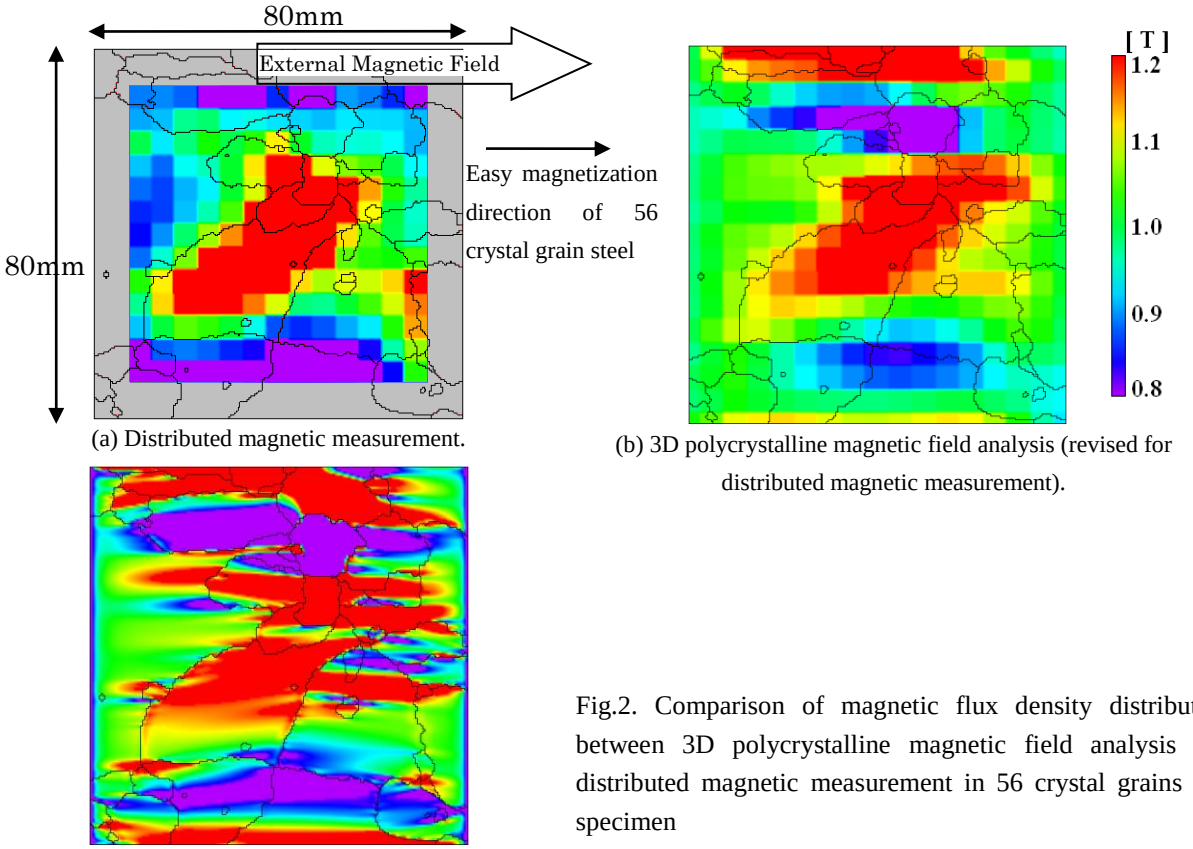

(a) Distributed magnetic measurement.

(b) 3D polycrystalline magnetic field analysis (revised for distributed magnetic measurement).

(c) 3D polycrystalline magnetic field analysis (original).

Fig.2. Comparison of magnetic flux density distribution between 3D polycrystalline magnetic field analysis and distributed magnetic measurement in 56 crystal grains GO specimen

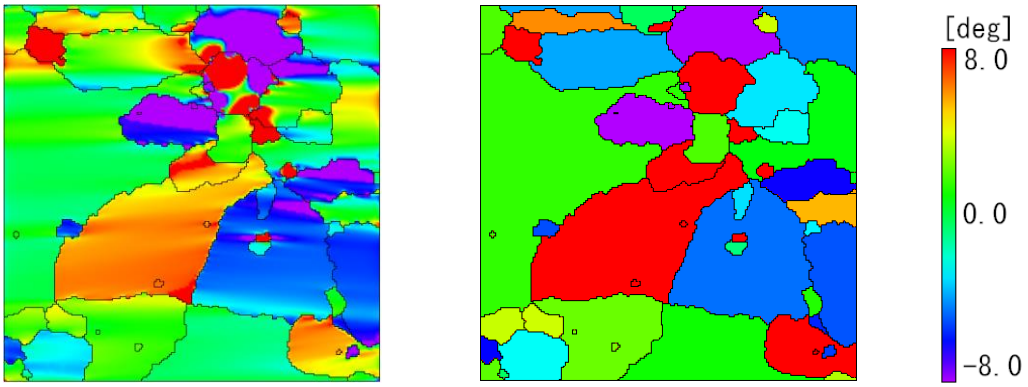

(a) 3D polycrystalline magnetic field analysis

(b) α angle distribution.

Fig.3. Comparison of inclination angle of magnetic flux density vector $\vec{B}$ between 3D polycrystalline magnetic field analysis and distributed magnetic measurement in 56 crystal grains GO specimen.

Reference

1) K. Fujisaki, S. Satoh, “Numerical calculations of electromagnetic fields in silicon steel under mechanical stress,” IEEE Trans. on Magn., Vol. 40, No.4, pp.1820–1825, (2004).
2) K. Fujisaki, M. Fujikura, J. Mino, S. Satou, “3-dimensional Magnetic Field Analysis by Homogenization Method for Thin Steel Plate,” Trans. D, IEEJ, Vol.128, No.3, pp.303-309, (2008).
3) K. Fujisaki, T. Tamaki, “Three-dimensional Polycrystal Magnetic Field Analysis of Thin Steel”, IEEE Transactions on Magnetics s, Volume 45, No.2, pp.687-693, February, (2009).
4) Keisuke Fujisaki, Teruyuki Tamaki, Shouichi Yasuhiro, “Comparison of 3D Polycrtystal Magnetic Field Analysis and Distributed Magnetic Measurement,” Trans. A, IEEJ, vol.129, no.11. pp. 821-826, 2009.

Harmonic Iron Loss Analysis of Rotating Machines: Practical Macro Modeling for Stress and Hysteresis

Katumi Yamazaki
(Chiba Institute of Technology)

In this symposium, I present harmonic iron loss analysis of rotating machines that considers effects of multi-axial mechanical stress and hysteresis phenomenon by introducing practical macro modeling.

First, the effect of the multi-axial stress on the loss is investigated by material experiments. An approximated modeling, which requires only the measured loss with uniaxial stress, is also introduced. Fig. 1 shows the experimental system [1], in which arbitrary 2-axial stress can be imposed on the specimen of an electrical steel sheet by the actuators noted 1 and 2. The magnetic field is applied along the direction of the force produced by actuator 1. The specimen is an electrical steel sheet with 3% silicon.

The hysteresis loss and the eddy current loss including the excess loss are separated from the measured total core losses at 50 Hz and 200 Hz. Fig. 2 shows the results. It is revealed that both the eddy current and hysteresis losses are affected by multi-axial stress. These losses become maximum when the compressive (minus) σ_1 and tensile (plus) σ_2 are imposed.

This experiment cannot be always carried out for practical design procedure of rotating machines. Approximated modeling is strongly desired. To obtain the approximated multi-axial stress effects, the single axial equivalent stress σ_{eq} has been proposed.

Following expression was derived under the assumption that a same magneto-elastic energy leads to a same characteristics of the magnetic materials [2]:

$$\sigma_{eq} = \frac{3}{2}\vec{h}.\boldsymbol{s}.\vec{h} \qquad (1)$$

where $\vec{h}$ is the unit vector along the magnetic field direction, $\boldsymbol{s}$ is the deviatoric part of the stress tensor expressed by σ_1 and σ_2. It is assumed that the variation in core loss with single σ_{eq} along the magnetic field direction is identical to that with multi-axial σ_1 and σ_2. Therefore, the effect of the multi-axial stress can be estimated only by (1) and the experiment, in which a uniaxial stress is simply imposed along the flux direction.

Fig. 3 shows the calculated variation in the losses only from the measured loss $W(\sigma_1,0)$ by single axial σ_1 and the equivalent stresses. It is confirmed that the calculated result well express the measured eddy current and hysteresis losses in Fig. 2.

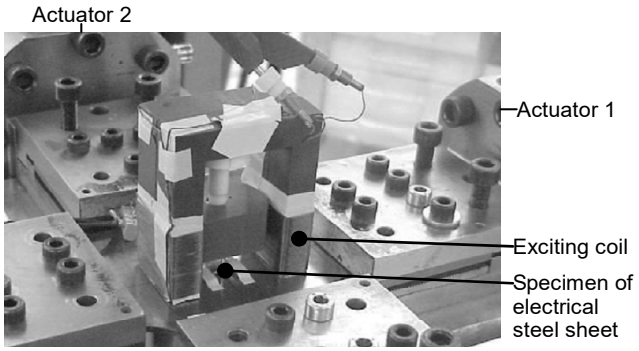

Fig. 1. Experimental system for effect of multi-axial stress[1].

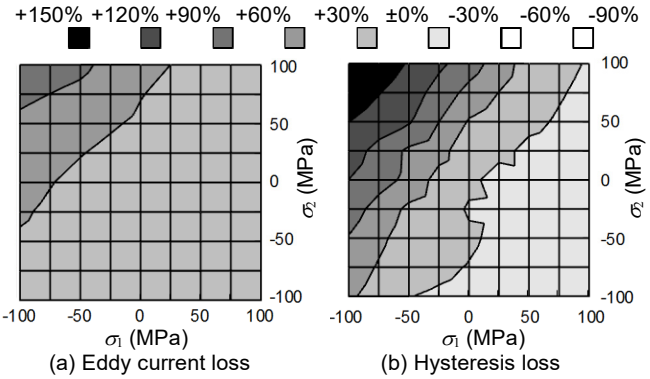

Fig. 2 . Measured variation in losses with multi-axial stress.

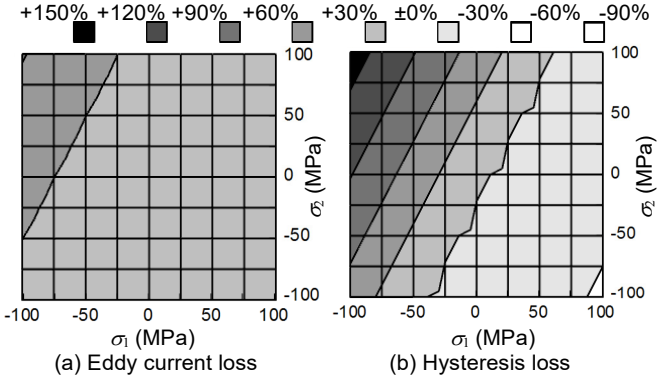

Fig. 3. Calculated losses by $W(\sigma_1,0)$ and σ_{eq} by (1)

Next, a practical hysteresis modeling including minor loops is proposed [3]. Fig. 4 shows the concept of this model. The minor loops are approximately determined form the several curves of major loops. Fig. 5 shows the experimental verification of this model by a single sheet test of an electrical steel sheet. The accuracy of the model is confirmed.

Finally, the proposed material modeling is applied to the loss calculation of a 100 kW class interior permanent magnet synchronous motor driven by a PWM inverter (5 kHz carrier). The 2D finite element analysis is carried out due to following equation.

$$\nabla \times \left(\frac{1}{\mu} \nabla \times \boldsymbol{A} \right) = \nabla \times \boldsymbol{H}_{eddy,ave} + \nabla \times \boldsymbol{H}_{hys,ave} \quad (2)$$

where μ is the permeability, $\boldsymbol{A}$ is the magnetic vector potential, $\boldsymbol{H}_{eddy,ave}$ and $\boldsymbol{H}_{hys,ave}$ are the reation field caused by the eddy currents and hysteresis phenomenon in the core, which are averaged along the thickness of electrical steel sheets. $\boldsymbol{H}_{eddy,ave}$ is determined by coupling 1D nonlinear time stepping analysis along the thickness of the electrical steel sheet in the core. $\boldsymbol{H}_{hys,ave}$ is determined by the presented hysteresis model by considering the effect of the stress due to (1).

Fig. 6 shows the calculated flux density waveform at the top of a stator tooth of the motor. The waveform includes high-frequency carrier harmonics. Fig. 7 shows the calculated hysteresis loops, which includes a considerable number of minor loops. It is observed that the differential permeability of the minor loops is considerably smaller than that of the B-H curve used in the conventional analysis. Fig. 8 shows the experimental and calculated iron losses. The accuracy is improved by the proposed method due to the correct estimation of skin effect.

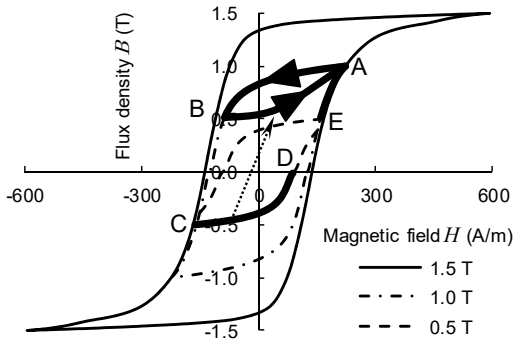

Fig. 4. Minor hysteresis loop modeling.

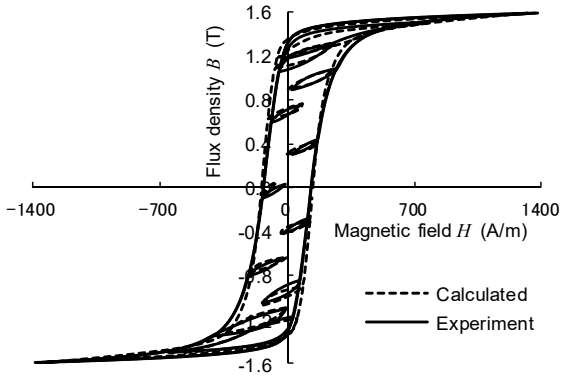

Fig. 5. Experimental verification of hysteresis modeling.

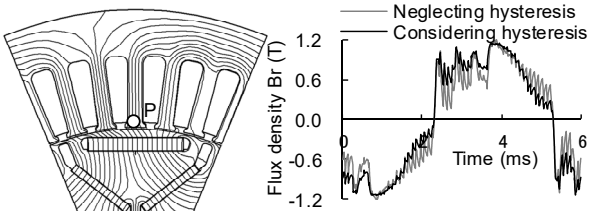

Fig. 6. Calculated flux density waveform (2500 r/min, 88A)

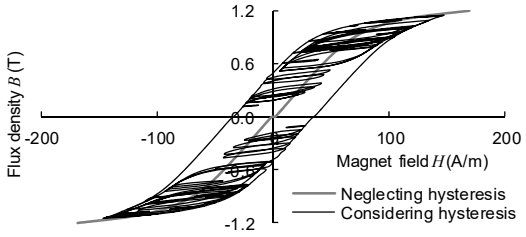

Fig. 7. Calculated hysteresis loop (2500 r/min, 88A).

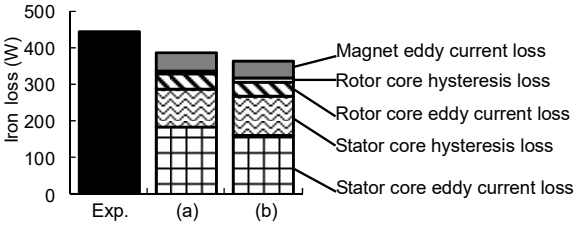

Fig. 8. Experimental and calculated iron losses (2500 r/min, 88A).
(a):Considering hysteresis, (b):Neglecting hysteresis

Reference

1) M. Rekik, O. Hubert, and L. Daniel, "Influence of a multiaxial stress on the reversible and irreversible magnetic behavior of a 3% Si-Fe alloy", *Int. J. Applied Electromagnetics and Mechanics*, vol. 44, no. 3, 4, pp. 301-315, 2014.

2) L. Daniel and O. Hubert, "An equivalent stress for the influence of multiaxial stress on the magnetic behavior," *J. Applied Physics*, vol. 105, 07A313, 2009.

3) K. Yamazaki and Y. Sakamoto, "Electromagnetic field analysis considering reaction field caused by eddy currents and hysteresis phenomenon in laminated cores," *IEEE Trans. Magn.*,vol.59, no. 3, 1300294, 2018.

Homogenization Techniques for Laminated Core and Soft Magnetic Composites in Magnetic Field Analysis

Kazuhiro Muramatsu
Department of Electrical and Electronic Engineering, Saga University, Saga 840-8502, Japan

1. Introduction

In electrical machines, laminated cores and soft magnetic composites (SMCs) are often used in order to reduce the eddy current losses. In the magnetic field analysis of such machines, the cores are usually modeled by solid ones in order to save computation cost. To take account of the nonlinearity and the eddy currents in steel plates or particles, and the gaps between them in the solid core model, homogenization techniques [1), 2)] are applied. In this paper, the homogenization techniques for laminated core and SMCs are described.

2. Homogenization Technique

The flowchart of the homogenization technique for laminated core or SMCs is shown in Fig. 1. The sub-analysis with the cell model of a steel plate or particle is carried out for each element *ie* in the core at each nonlinear iteration in the 3D nonlinear eddy current analysis with the solid core model ("main-analysis"). In the sub-analysis, the flux densities obtained from the main analysis are given and the effective permeability used in the main analysis is calculated taking account of the nonlinearity, the eddy currents, and the gaps.

3. Laminated Core

In the sub-analysis of the homogenization technique for the laminated core, one sheet of steel plate with the gap is chosen as the cell model, shown in Fig. 2, and the 1D nonlinear eddy current analysis is carried out.

The homogenization technique is applied to a simple reactor model [3)] shown in Fig. 3. The cores with gaps are constructed by laminated steel plates (35A270) in the *z*-direction, and the space factor *F* is 0.95.

The flux distributions in the leg in the *y*-*z* plane obtained from the ordinary method, neglecting the eddy currents in the steel plates and gaps between the steel plates, and the proposed method mentioned above are shown in Fig. 4. The flux distribution obtained from the ordinary method is almost uniform in the core, whereas the flux densities in the upper layers of the core are larger than those in the other lower layers in the proposed method. This is because the flux concentrates at the corners of cores due to the gaps between cores and the larger flux in the upper layers remains due to the gaps between the steel plates. Therefore, the proposed method should be used for the accurate

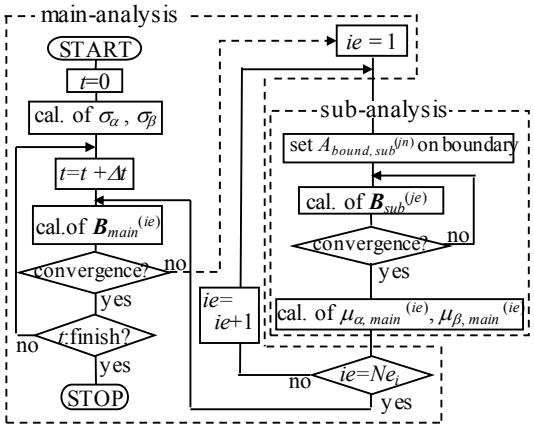

Ne_i : number of elements in core in main-analysis

Fig. 1 Flowchart of homogenization technique.

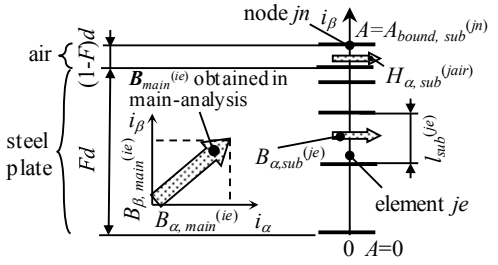

Fig. 2 1D cell model of a steel plate in laminated core.

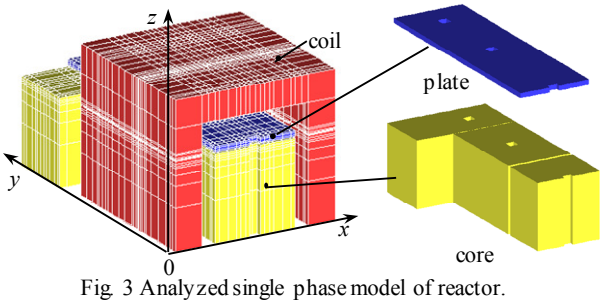

Fig. 3 Analyzed single phase model of reactor.

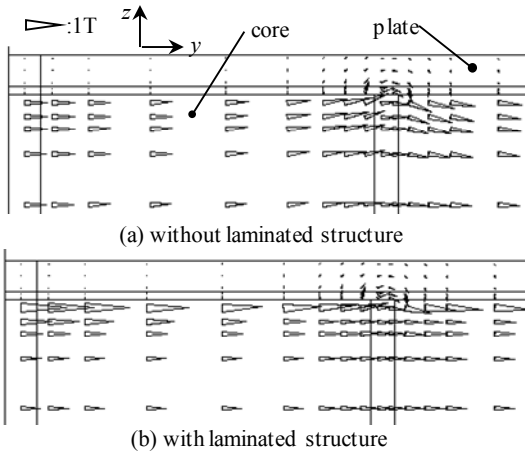

(a) without laminated structure

(b) with laminated structure

Fig. 4 Flux distributions in the leg

analysis of the laminated core.

4. Soft Magnetic Composites (SMCs)

To establish the homogenization technique for SMC, the accurate cell model of a particle with gap is investigated[4]. Fig. 5 shows a 3D cell model for an actual SMC (MBS-R3, DIAMET CORPORATION). In this model, the particles are assumed to be square shape and be formed regularly and infinitely. Two configurations of particles with uniform and un-uniform gaps are examined as shown in Fig. 5 (a) and (b), respectively. In the model with the uniform gap, two gap lengths G_0s are selected. One is G_0s = 1.37 μm determined by volume filling rate. The other is set to be G_0 = 0.35 μm so that the calculated magnetic field H_z coincides with measured one at B_z = 1T. In the non-uniform gap model, G_1, G_2, and L in Fig 1 (b) are optimized to be 0.15, 1.0, and 35 μm so that the calculated BH curve coincides with the measured one as possible.

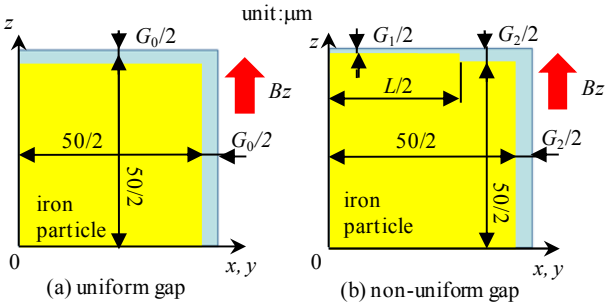

Fig. 5 3D Cell model of a particle in SMC.

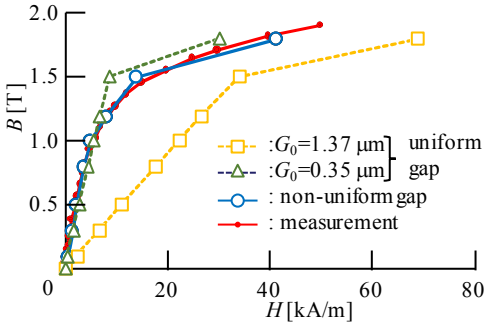

Fig. 6 Calculated and measured initial BH curves.

Fig. 6 shows the calculated and measured effective initial BH curves in the low frequency in which the eddy current can be neglected. In the model with uniform gap G_0 = 1.37 μm, the calculated effective permeability is much smaller than the measured one because the gap length determined by the filling ratio is larger than most of those in the actual SMC due to its complex shape of particles. The model with the smaller uniform gap G_0 = 0.35 μm cannot represent the measured BH curve completely, too. The BH curve obtained by the optimized model with non-uniform gap is good agreement with the measured one. It can be concluded that the cell model with non-uniform gap should be used for the homogenization technique of SMC.

Fig. 7 shows the comparison of the calculated iron losses obtained by using the cell model shown in Fig. 5 (a) with the measred ones. The calculated hysteresis losses are in good agreement with the measured ones because the applied flux density coincides with each other. However, the eddy current losses are different from measured ones because the insulation between particles are not completed in an actual SMCs. This problem will be investigated in future.

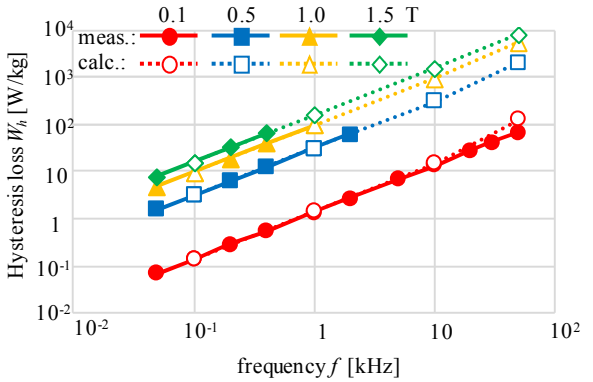

(a) hysteresis loss

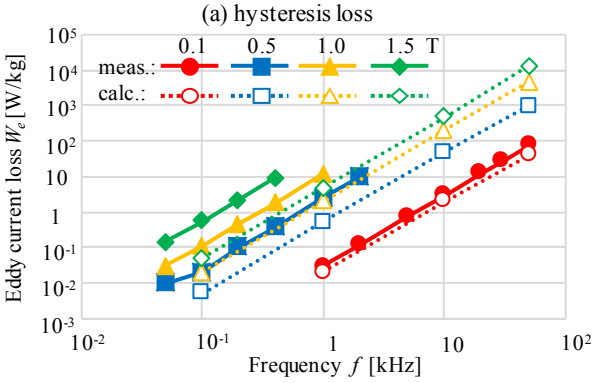

(b) eddy current loss

Fig. 7 Iron losses.

References

1) K. Muramatsu, et al., *IEEE Trans. Magn.*, vol. 40, no. 2, pp. 896-899, 2004.
2) Y. Sato, et al., *IEEE Trans. Magn.*, vol. 53, no. 6, Art. no. 7402204, 2017.
3) Y. Gao, et al., *IEEE Trans. Magn.*, vol. 45, no. 3, pp. 1044-1047, 2009.
4) Y. Gao, et al., *IEEE Trans. Magn.*, vol. 54, no. 3, Art. no. 7401504, 2018.

Magnetic Material Modeling and Simulation Technology for Loss Calculation

A. Furuya, Y. Uehara, K. Shimizu, J. Fujisaki, T. Ataka, T. Tanaka, H. Kawano* and H. Oshima*
(Fujitsu Ltd., *Fujitsu Laboratories Ltd.)

Soft magnetic materials such as an electrical steel, ferrite core, and dust core are widely used in an inductor and transformer. To achieve high efficiency and downsizing, a simulation technology for accurate core loss is highly demanded in the industry. However, core loss is strongly related to complex magnetization dynamics, and magnetic material modeling is one of the recent fields in which progress is being made. In this presentation, we introduce a magnetic material modeling technique based on micromagnetics for electrical steel, and microstructure for ferrite core.

For electrical steel, hysteresis loss accounts for a large portion of core loss of motors. In addition, vector property due to grain structure is observed in B-H loop measurement. To model this property, we adopted a grain magnetics (GM) model[(1)]. Fig. 1 shows the conceptual diagram of the GM model. The magnetization of one grain is approximated by one magnetization vector. This formulation cannot treat a domain-wall and its related dynamics, and therefore, artificial magnetization change such as magnetization flip is introduced. Fig. 2 shows the simulation results for grain-oriented electrical steel. Anisotropic B-H loops are well-reproduced by considering the effect of domain-wall motion and crystal anisotropy.

For high frequency applications, soft ferrite cores are an important material, but these core losses are strongly related to eddy-current, dimensional resonance, and excess loss due to the magnetization dynamics. To evaluate core loss of Mn-Zn ferrite, we studied the magnetic field simulation with the effective permittivity that comes from the microstructure of Mn-Zn ferrite[(2)]. Fig. 3 shows the simulation result of core-size dependence of complex permeability. The core sample with diameter size 12.7 mm has a clear peak in its real part due to the dimensional resonance. In this presentation, we will discuss the comparison of core loss with experimental measurement and loss mechanism.

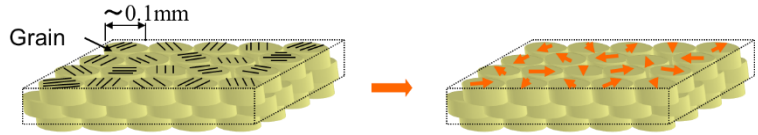

Fig. 1: Grain magnetics model for electrical steel

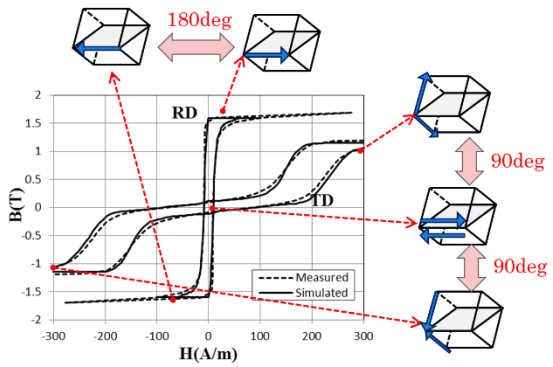

Fig. 2: B-H loops of grain-oriented electrical steel

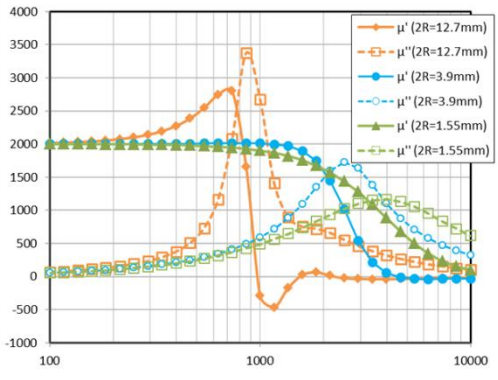

Fig. 3: Complex permeability of Mn-Zn core

Reference

1) A. Furuya,J. Fujisaki,Y. Uehara,K. Shimizu,H. Oshima, and T. Matsuo, IEEE Trans. on Magn., vol. 50,(2014),7300604
2) A. Furuya, Y. Uehara, K. Shimizu, J. Fujisaki, T. Ataka, T. Tanaka and H. Oshima", IEEE Trans. on Magn., vol. 53,(2017), 7301004

Magnetic properties and variational calculus

Fumiaki Ikeda
Photon Co., Ltd.

The finite element method is currently the mainstream method in the field of low frequency electromagnetic field analysis. In this method, Maxwell's equation, which is a fundamental equation, is formulated using a weighted residual method such as the Galerkin method. This is because the magnetization characteristics of magnetic materials are generally not linear with constant magnetic permeability, but have a nonlinear dependence on magnetic flux density.

In the case of a linear magnetic material, the fundamental equation can be expressed as follows using the variational calculus.

$$\delta \int_V [\frac{1}{2\mu}(\mathrm{rot}\boldsymbol{A})^2 - \boldsymbol{J}\cdot\boldsymbol{A}]dV = 0 \tag{1}$$

Here μ is permeability and has a constant value. $\boldsymbol{A}$ is vector potential, and $\boldsymbol{J}$ is current density. Taking variations, the left-hand side becomes as follows.

$$\begin{aligned}&\int_V [\frac{1}{\mu}\mathrm{rot}\delta\boldsymbol{A}\cdot\mathrm{rot}\boldsymbol{A} - \delta\boldsymbol{A}\cdot\boldsymbol{J}]dV \\ &= \int_V \delta\boldsymbol{A}\cdot[\mathrm{rot}\frac{1}{\mu}\mathrm{rot}\boldsymbol{A} - \boldsymbol{J}]dV + \text{(Surface integral)}\end{aligned} \tag{2}$$

However, since the transformation of the last formula was performed using Gauss' theorem, a surface integral has appeared. Since this surface integral normally disappears through boundary conditions, it is required that the integral of the first term be zero, and it is possible to solve the electromagnetic field equation by the variational calculus.

However, in general magnetic materials, the magnetic permeability is not constant, and so such variational calculus cannot be used. Therefore, when dealing with these kinds of magnetic materials using the finite element method, we utilize the vector weighting function $\boldsymbol{W}$ to produce the following equation.

$$\int_V \boldsymbol{W}\cdot[\mathrm{rot}\frac{1}{\mu}\mathrm{rot}\boldsymbol{A} - \boldsymbol{J}]dV = 0 \tag{3}$$

If the left-hand side can be transformed using Gauss' theorem and the surface integral eliminated through boundary conditions, the formula becomes as follows.

$$\int_V [\frac{1}{\mu}\mathrm{rot}\boldsymbol{W}\cdot\mathrm{rot}\boldsymbol{A} - \boldsymbol{W}\cdot\boldsymbol{J}]dV = 0 \tag{4}$$

In this study, we show that the variational calculus can be used even for general magnetic materials by considering the thermodynamics of the magnetic material, and demonstrate that, in electromagnetic field analysis also, the finite element method can be formulated naturally.

Considering the free energy F of the magnetic material as a function of temperature T and magnetic flux density $\boldsymbol{B}$, this differential can be expressed as follows.

$$dF(T,\boldsymbol{B}) = -SdT + \boldsymbol{H}\cdot d\boldsymbol{B} \tag{5}$$

Here, S is the entropy of the magnetic material per unit volume, T is temperature, and $\boldsymbol{H}$ is magnetic field. From this, the thermodynamic variables can be expressed as follows.

$$\begin{aligned}S &= -\frac{\partial}{\partial T}F(T,\boldsymbol{B}) \\ \boldsymbol{H} &= \frac{\partial}{\partial \boldsymbol{B}}F(T,\boldsymbol{B})\end{aligned} \tag{6}$$

Here we introduce the following thermodynamic potential by transforming variables.

$$G(T, \boldsymbol{H}) = F(T, \boldsymbol{B}) - \boldsymbol{H} \cdot \boldsymbol{B} \tag{7}$$

Calculating this derivative, the following is obtained from Eq. (5).

$$dG(T, \boldsymbol{H}) = -SdT - \boldsymbol{B} \cdot d\boldsymbol{H} \tag{8}$$

In electromagnetic field analysis, the magnetic field is often obtained by inputting a current, which corresponds to the problem of finding the magnetic flux density for a magnetic field $\boldsymbol{H}$ generated by an electric current. According to thermodynamics, for fixed temperature and magnetic field, this temperature thermodynamic potential is at its minimum at equilibrium. Therefore, the variation of the following integral must be zero if temperature is constant.

$$\delta \int_V G(T, \boldsymbol{H}) dV = 0 \tag{9}$$

Since temperature and magnetic field are here assumed to be fixed, this variation is taken on magnetic flux density, which is the other state quantity. The variation on the left-hand side of this equation is calculated as follows.

$$\begin{aligned} &\int_V [\frac{\partial}{\partial \boldsymbol{B}} F(T, \boldsymbol{B}) \cdot \delta \boldsymbol{B} - \boldsymbol{H} \cdot \delta \boldsymbol{B}] dV \\ &= \int_V dV \delta \boldsymbol{B} \cdot [\frac{\partial}{\partial \boldsymbol{B}} F(T, \boldsymbol{B}) - \boldsymbol{H}] dV \end{aligned} \tag{10}$$

When the variations are represented by vector potentials,

$$\delta \boldsymbol{B} = \delta \mathrm{rot} \boldsymbol{A} = \mathrm{rot} \delta \boldsymbol{A} \tag{11}$$

The above left-hand side can be further transformed as follows through partial integration using Gauss' integral theorem.

$$\begin{aligned} &\int_V dV \mathrm{rot} \delta \boldsymbol{A} \cdot [\frac{\partial}{\partial \boldsymbol{B}} F(T, \boldsymbol{B}) - \boldsymbol{H}] dV \\ &= \int_V dV \delta \boldsymbol{A} \cdot \mathrm{rot} [\frac{\partial}{\partial \boldsymbol{B}} F(T, \boldsymbol{B}) - \boldsymbol{H}] dV + \text{(Surface integral)} \end{aligned} \tag{12}$$

Since the terms of the surface integral can be eliminated by appropriate boundary conditions, the above equation becomes as follows.

$$\int_V dV \delta \boldsymbol{A} \cdot [\mathrm{rot} \frac{\partial}{\partial \boldsymbol{B}} F(T, \boldsymbol{B}) - \mathrm{rot} \boldsymbol{H}] dV \tag{13}$$

Although the distribution of the magnetic field cannot be determined, the magnetic field within this integral is subject to a rotation operator, and can be converted into current density as follows.

$$\mathrm{rot} \boldsymbol{H} = \boldsymbol{J} \tag{14}$$

Therefore, the equation obtained from the variational calculus for the thermodynamic potential, which is required from thermodynamics, is as follows.

$$\int_V dV \delta \boldsymbol{A} \cdot [\mathrm{rot} \frac{\partial}{\partial \boldsymbol{B}} F(T, \boldsymbol{B}) - \boldsymbol{J}] dV = 0 \tag{15}$$

From equation (6), we can see that this formula is equivalent to the electromagnetic field analysis equation.

Here, by examining the magnetic material thermodynamically, we have shown that magnetization characteristics can be expressed by thermodynamic potentials such as free energy, and that the variational calculus can be used in the finite element method for the electromagnetic field.

Issues of Material Modeling in Electromechanical Simulations

Takashi Yamada[1], Katsuyuki Narita[1], Hiroyuki Sano[1]
([1]JMAG division, JSOL Corp.)

Many electrical devices are re-designed today in the electrification. Since the electrification is mainly for energy saving or the global warming countermeasures, high energy efficiency is primary requirement of the re-design. A typical example is electric motors of electric vehicles which have to have high energy efficiency as well as high power density with which the conventional internal combustion engines must be able to be replaced.

On the other hand, the further improvement is challenging since such electric machines have long history of over 100 years and countless efforts have been already made in the history. In order to make a breakthrough, advanced simulation technologies such as finite element analysis (FEA) has been introduced and recognized as an indispensable tool in the machine developments. Major advantages of FEA are, firstly, virtual prototyping where any design ideas can be concretely implemented and evaluated and, secondly, detail phenomena in a machine are visualized and investigated. Those advantages give us deep insights in a complex system and substantial improvements which are difficult with conventional design approaches consisting of empirical equations and real prototyping.

However, to enjoy the advantages, the simulation has to have enough accuracy. Since main error source of today's FEA is material data, accuracy of the material modeling determines performance of the simulation. Hereafter, we focus on losses of lamination steel which is used for core of the electric machines and its property largely affects the performance of the machines. More importantly, the property of the lamination steel is complex and difficult to be modeled so that we have many remaining issues there.

The losses of the lamination steel consist of hysteresis loss, eddy current loss and excess loss. The hysteresis loss is a loss defined by loops of static BH characteristic, i.g. it is frequency independent. The eddy current loss is caused by the classical eddy current circulating in a cross section which is perpendicular to main linkage flux direction. The excess loss is defined as a difference between total losses and summation of the hysteresis loss and eddy current loss.

Most common modeling approaches for loss evaluation today employ an empirical formula such as Steinmetz's equation in which coefficients and parameters are determined with measurements. The measurements are usually done with a pure sinusoidal waveform of magnetic flux density. Advantages of the conventional approach are, firstly, it is accurate if the actual operating condition is the same as the condition of measurements determining the coefficients of the formula and, secondly, it is simple to use since the total loss is calculated with a single formula which includes all losses in the above.

Disadvantage of the conventional approach is the fact that accuracy is never be guaranteed if the measurement condition does not match to the actual operating condition. Those undesirable situations are not rare in actual machines, especially, in advanced machines such as a traction motor of EVs. Those advanced machines are fed with higher current than of the conventional machines to achieve high power density so that the lamination steel is magnetically highly saturated and this does not satisfy the measurement condition. Also, those advanced machines are controlled with inverter(s) employing Pulse Width Modulation (PWM) technique which generates high frequency minor loops on a fundamental major loop. The measurement condition does not include the minor loops and the resulting losses cannot represent the minor loop losses. The minor loops are generated not only by PWM but also by slot harmonics in a Permanent Magnet Synchronous Machine (PMSM) which is the main stream in EVs. Moreover, the measurement has limitation in frequency which actual frequency in a machine goes above the limitation. The disadvantage was not a significant problem because classical machines are designed to be operated with the low frequency sinusoidal waveforms of magnetic flux density.

To overcome the disadvantage, new models have been introduced for the hysteresis loss and the eddy current loss. The hysteresis loss is represented with Play-Hysteron model[1)] which is a semi-physical model and can reproduce a minor loop at an arbitrary operation point employing multiple static major loops. The eddy current loss is modeled by 1D-FEM[1)] in which eddy current distribution in thickness direction is solved with a conductivity of the steel sheet by one-dimensional FEM at each element of the main 2D/3D FEM. Note that since only conductivity is required, this method is valid for any frequency without limitation. Those two models give us significant improvements in accuracy for the advanced machines[3)]. A significant difference from the conventional approach is the fact that the new approach does not depend on measured losses and has wider applicability than the conventional approach.

However, the new approach misses the excess loss is inaccurate in case the excess loss is not ignorable. Although the best way to incorporate the excess loss is having a physical model, the phenomena are too complex to capture the mechanism. Currently, we are developing an expandable empirical based model as a second best. The new model shows reasonable performance for wide range even outside of the measurements. The detail will be explained in the presentation.

Reference

1) T. Matsuo, D. Shimode, , Y. Terada, M. Shimasaki ,"Application of stop and play models to the representation of magnetic characteristics of silicon steel sheet", IEEE Transactions on Magnetics, vol.39, no.3, pp. 1361-1364, 2003
2) O. Bottauscio, “Advanced Model of Laminated Magnetic Cores for Two-Dimensional Field Analysis”, IEEE Transactions on Magnetics, vol.36, no.3, pp561-573, 200
3) K. Narita, H. Sano, T. Yamada, K. Aiso, K. Akatsu, “An Accurate Iron Loss Evaluation Method Based on Finite Element Analysis for Switched Reluctance Motors”, ECCE 2015

Equivalent circuit for Eddy Current Field in Cauer Form

Y. Shindo[1] and T. Matsuo[2]
[1]Kawasaki Heavy Industries, Akashi 673-8666, Japan
[2]Kyoto University, Kyoto 615-8520, Japan

Recently, an exact and efficient modeling method for the eddy current field is found.[1)] This method expands the eddy current field to an equivalent circuit called Cauer Ladder Network (CLN). The procedure for obtaining this network and the benefits of this method are introduced here.

Consider a magnetic sheet shown in Fig. 1, where d denotes the width of the sheet, μ and σ denote the magnetic permeability and electric conductivity of the material respectively. It is supposed that exciting field $\dot{H}_0$ is applied externally. The equation for the eddy current field is given by (1) as an one-dimensional problem.

$$\frac{\partial^2 \dot{H}(x)}{\partial x^2} - j\omega\sigma\mu\dot{H}(x) = 0 \quad . \tag{1}$$

Solving this equation under the boundary condition $\dot{H}(d/2) = \dot{H}_0$ gives the magnetic field (2) and the equivalent magnetic permeability as (3).

$$\dot{H}(x) = \frac{\cos(kx)}{\cos(kd/2)}\dot{H}_0 \tag{2}$$

$$\dot{\mu} = \frac{\dot{\Phi}}{d\dot{H}_0} = \mu\frac{2}{kd}\tan\left(\frac{kd}{2}\right), \qquad \dot{\Phi} = \int_{-d/2}^{d/2}\mu\dot{H}(x)\,\mathrm{d}x = \frac{2\mu}{k}\tan\left(\frac{kd}{2}\right)\dot{H}_0 . \tag{3}$$

Here the complex variable k is defined by $k = \sqrt{-j\omega\sigma\mu}$ and $\dot{\Phi}$ denotes the total flux in the magnetic sheet. The trigonometric function divided by its argument can be expanded by the following two forms, a partial fraction expansion (4) and a continued fraction (5).

$$\frac{1}{z}\tan z = -2\sum_{n=1}^{\infty}\frac{1}{z^2 - \left[(2n-1)\pi/2\right]^2} \tag{4}$$

$$\frac{1}{z}\tan z = \cfrac{1}{1-\cfrac{z^2}{3-\cfrac{z^2}{5-\cfrac{z^2}{7-\cfrac{z^2}{9-\cdots}}}}} \tag{5}$$

By setting $R_c = 8/\sigma d^2$, $L_c = \mu$ and $L_{cn} = 2L_c/(n-1/2)^2\pi^2$, the effective complex permeability can be respectively expanded as

$$j\omega\dot{\mu} = \sum_{n=1}^{\infty}\frac{j\omega L_{cn}R_c}{R_c + j\omega L_{cn}} \tag{6}$$

$$j\omega\dot{\mu} = \cfrac{1}{1/j\omega L_c + \cfrac{1}{3(R_c/2) + \cfrac{1}{5/j\omega L_c + \cfrac{1}{7(R_c/2) + \cdots}}}} . \tag{7}$$

The former corresponds to the Fourier I expansion and the latter corresponds to the Cauer I expansion. The equivalent circuits for these expansions can be realized by the equivalent circuits shown in Fig. 2, Foster realization and Cauer realization respectively. These equivalent circuits can be employed for modeling of actual electric machines such as a reactor as shown in Fig. 3. In fact, the reactance of this reactor is expressed by $\mathrm{j}\omega L = \mathrm{j}\omega\dot{\mu}SN/l$, where S, N and l

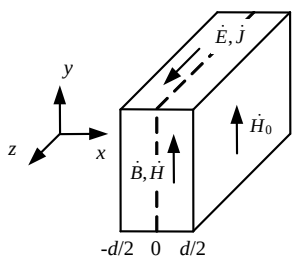

Fig. 1. Magnetic sheet

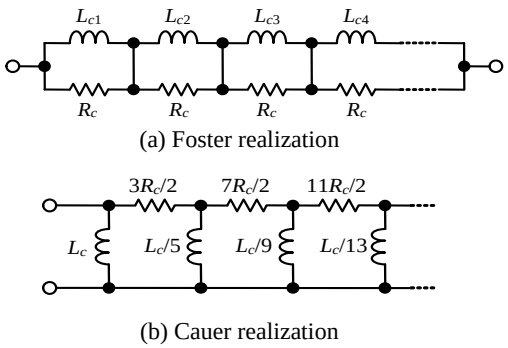

(a) Foster realization

(b) Cauer realization

Fig. 2. Equivalent circuits

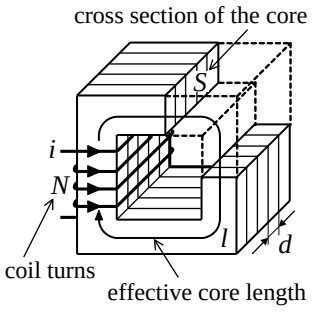

Fig. 3 Reactor

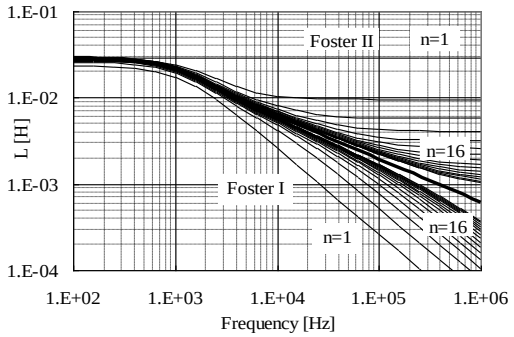

(a) Foster I and II

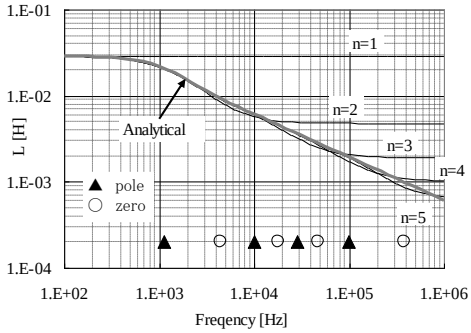

(b) Cauer I

Fig. 4. Bode plots of Foster and Cauer expansions. ($L = \dot{\mu}$)

denote the cross section of the laminated core, the coil turns and the effective core length respectively. The examples of Bode plots with finite truncations of these networks are shown in Fig 4, where *n* denotes the number of the inductors. It is obvious that Cauer expansion is much effective than Foster expansion.

Recently, it was found that this Cauer realization can be expanded to arbitrary three-dimensional eddy current field as illustrated in Fig. 5.[2] For preparation, define

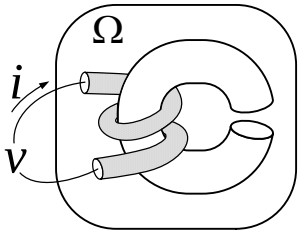

Fig. 5. Eddy current field

$$\boldsymbol{E} = \sum_{n=0}^{\infty} e_{2n}\bar{\boldsymbol{E}}_{2n}, \quad \boldsymbol{H} = \sum_{n=0}^{\infty} h_{2n+1}\bar{\boldsymbol{H}}_{2n+1}, \tag{8}$$

$$1/R_{2n} = \int_{\Omega} \sigma \bar{\boldsymbol{E}}_{2n} \cdot \bar{\boldsymbol{E}}_{2n} \mathrm{d}V, \quad L_{2n+1} = \int_{\Omega} \mu \bar{\boldsymbol{H}}_{2n+1} \cdot \bar{\boldsymbol{H}}_{2n+1} \mathrm{d}V . \tag{9}$$

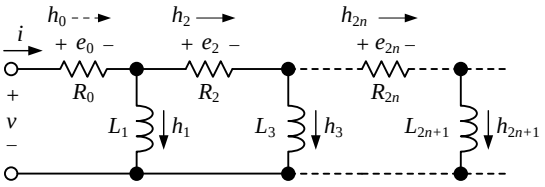

Fig. 6. Ladder network

Then the method is presented by the following steps.

***Step* 0**: Assume that the voltage *v* is applied externally. Solve $\nabla \times \boldsymbol{E}_0 = 0$ under given voltage boundary condition. Set $\bar{\boldsymbol{E}}_0 = \boldsymbol{E}_0 / v$ and calculate R_0 using (9). Set $\bar{\boldsymbol{H}}_{-1} = 0$ and n = 1.

***Step* 1**: Solve $\nabla \times \tilde{\boldsymbol{H}}_{2n-1} = R_{2n-1}\sigma \bar{\boldsymbol{E}}_{2n-2}$ under magnetic boundary conditions. Set $\bar{\boldsymbol{H}}_{2n-1} = \tilde{\boldsymbol{H}}_{2n-1} + \bar{\boldsymbol{H}}_{2n-3}$ and calculate L_{2n-1} by using (9).

***Step* 2**: Solve $\nabla \times \tilde{\boldsymbol{E}}_{2n} = -(1/L_{2n-1})\mu \bar{\boldsymbol{H}}_{2n-1}$. Set $\bar{\boldsymbol{E}}_{2n} = \tilde{\boldsymbol{E}}_{2n} + \bar{\boldsymbol{E}}_{2n-2}$ and calculate R_{2n} by using (9).

***Step* 3**: If the finite sum of (8) converge sufficiently, then stop the calculation. Otherwise set $n = n+1$ and go to ***Step* 1**.

This method provides the network constants in Fig. 6, and simultaneously provides the spatial distribution functions $\bar{\boldsymbol{E}}_{2n}$ and $\bar{\boldsymbol{H}}_{2n+1}$. The circuit variables e_{2n} and h_{2n+1} can be obtained by real-time simulation of the ladder network. The magnetic field and the current distribution can be synthesized using (8). Furthermore, the total magnetic energy W_m and the power consumption W_R in the entire domain Ω are presented in lumped forms as

$$W_m = \frac{1}{2}\sum_{n=0}^{\infty} L_{2n+1} h_{2n+1}^2, \quad W_R = \sum_{n=0}^{\infty} R_{2n} \left(\sum_{m=n}^{\infty} h_{2n+1} \right)^2 . \tag{10}$$

In the actual electric machine designs, the nonlinearity and hysteresis property, as well as the anomaly eddy current loss, frequently become important issues. [3] The authors hope that the proposed method can be applied to estimate the anomaly eddy current loss. However, it may not be so easy because of the moving of domain walls due to the fluctuation of the magnetic field.

Reference

1) Y. Shindo *et al*., Simple Circuit Simulation Models for Eddy Current in Magnetic Sheets and Wires, IEEJ Trans. FMS, Vol. 134, Issue 4, pp.173-181 (2014)
2) A. Kameari *et al*., Cauer Ladder Network Representation of Eddy-Current Fields for Model Order Reduction Using Finite-Element Method, IEEE Tran MAG, Vol. 52, Issue 3, #7201804 (2018)
3) G. Bertotti, Hysteresis in Magnetism, Academic Press (1998).